Univerzita Karlova v Praze
Matematicko-fyzikální fakulta

DIPLOMOVÁ PRÁCE

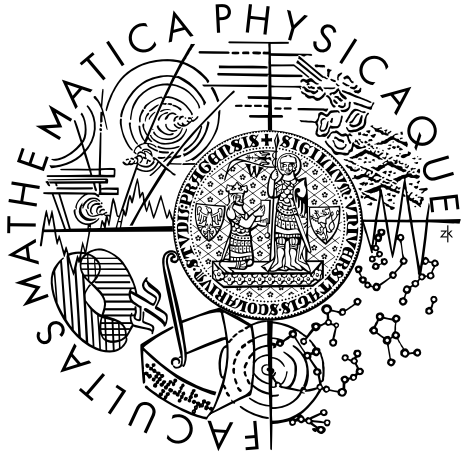

Bc. Lucia Mészárosová

Modernizace vnitřního detektoru ATLAS

Ústav částicové a jaderné fyziky

Vedoucí diplomové práce:	doc. RNDr. Zdeněk Doležal, Dr.
Studijní program:	Fyzika
Studijní obor:	Jaderná a subjaderná fyzika

Praha 2016

Charles University in Prague
Faculty of Mathematics and Physics

MASTER THESIS

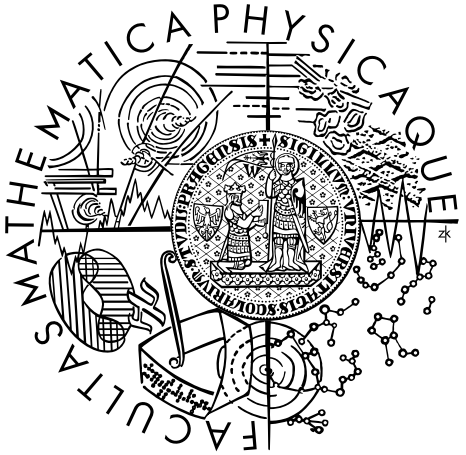

Bc. Lucia Mészárosová

The ATLAS Inner Detector Upgrade

Institute of Particle and Nuclear Physics

Supervisor of the master thesis:	doc. RNDr. Zdeněk Doležal, Dr.
Study programme:	Physics
Study branch:	Nuclear and Particle Physics

Prague 2016

I declare that I carried out this master thesis independently, and only with the cited sources, literature and other professional sources.

I understand that my work relates to the rights and obligations under the Act No. 121/2000 Sb., the Copyright Act, as amended, in particular the fact that the Charles University in Prague has the right to conclude a license agreement on the use of this work as a school work pursuant to Section 60 subsection 1 of the Copyright Act.

In Prague 13.5.2016

Title: The ATLAS Inner Detector Upgrade

Author: Bc. Lucia Mészárosová

Institute: Institute of Particle and Nuclear Physics

Supervisor: doc. RNDr. Zdeněk Doležal, Dr., Institute of Particle and Nuclear Physics

Abstract: The main goal of this master thesis is, at first, to describe upcoming upgrade of ATLAS experiment in CERN in Switzerland and to describe the principle of strip silicon detectors. Then it is measurement and analysis of data from laser tests with two lasers: red and infra-red. Last but not least goal is to document the method of measurement and analysis of laser tests for the future laser tests. The text of the thesis is divided into five chapters. The first chapter is dedicated to the research facility CERN, its present experiment ATLAS and future experiment ATLAS Upgrade. The second chapter explains properties of semiconductors and the principle of strip semiconductor detectors. The third chapter describes whole measurement layout: a lab for testing, equipment needed for the tests and the whole system functioning. In the fourth chapter there are actual results from the laser tests. The tests were done on two end-cap prototype modules for ATLAS Upgrade with strip silicon sensors using two lasers: red and infra-red. The last chapter briefly explains the functions of macros that were created for measuring and analysing data from laser tests.

Keywords: ATLAS, tracking detector, semiconductor detectors

I would like to thank doc. RNDr. Zdeněk Doležal, Dr. for the possibility to make this thesis, for all the advices, comments and patience throughout the entire process. I would like to acknowledge and thank RNDr. Peter Kodyš, CSc. for his help in the lab and for the comments for the measurements and analysis. I also would like to thank Bc. Martin Sýkora for his work at his bachelor thesis which made to make the motion stages functional which helped me with my measurements.

Contents

Introduction

In Swiss CERN accelerator LHC has been working for a few years since 2008. During its operation many successes were achieved, one of them is the discovery of Higgs boson.

Because of the success, the LHC definitely earned an opportunity to continue its research. In the future it will be upgraded to increased luminosity which will bring a new area of searching for the new physics and will widen the possibilities for the study of the characteristics of Higgs boson. Its name will be High Luminosity LHC (HL-LHC).

With increased luminosity, current LHC's detectors are not suited for this kind of environment. That means that also the ATLAS detector will have to be upgraded. The upgraded ATLAS detector will be given a new name: ATLAS Upgrade. The upgrade will affect all parts of it. The focus on this thesis will be the inner detector, specifically semiconductor strip detectors. Current status of preparation for ATLAS Upgrade is that prototypes are being made and tested.

In this thesis the prototypes for ATLAS Upgrade, specifically inner's detector strip silicon detectors, will be tested with laser. For the measurements two prototype were available.

The thesis focuses mainly on the laser tests of two prototype modules with end-cap strip silicon detectors and the results. The tests were done at IPNP in Prague. Measurements and analysis of results were done by the author of the thesis.

The thesis is separated into 5 chapters. The first chapter describes current and future ATLAS detector mainly focusing on their differences. The second chapter describes principle and function the semiconductor detectors. All the following chapters describe the measurements of properties of prototype modules. In the third chapter the places and equipment for the tests are described. In the fourth chapter there are all the results of laser tests. The fifth chapter describes used macros for measurement and analysis of data.

1. CERN and ATLAS

1.1 CERN

CERN is according to [1] abbreviation of a French name *"Conseil Européen pour la Recherche Nucléaire"* which means European Organization for Nuclear Research. It was founded in 1954 with an objective to do a world-class nuclear physics in Europe. They focused only on nuclear physics back then because the research concentrated to understanding the inside of the atom. Nowadays the research contains nuclear physics as well but mainly focuses on particle physics.

CERN is located on Swiss-French borders in Swiss Geneva. CERN has currently got 21 members, two of them are also Czech and Slovak Republic which joined CERN in 1992 together as Czechoslovakia and since 1993 they are part of CERN as 2 different member states. There are also non-member states participating in the research.

This organization is known by many discoveries like discovering Z and W intermediate bosons or the birth of the World Wide Web. The latest big discovery is detecting the Higgs boson. As a result of this discovery Peter Higgs and François Englert were given the Nobel prize in 2013.

There are many unique facilities at CERN. The most known is probably LHC (*Large Hadron Collider*). This collider was built in tunnel of previous accelerator LEP (*Large Electron Positron Collider*). LHC is a circular accelerator with length of 27 km with many magnets and accelerating structures. LHC started working in 2008, during the first run it started on energy 7 TeV (3.5 TeV per beam), rising to 8 TeV. The first run ended in 2013 and for the next two years (2013-2015) LHC was maintained and upgraded. Recently (spring 2015) LHC started to collide on energy 13 TeV [2].

LHC collides mainly two protons, few months a year it collides heavy ions. Protons (ions) are not injected directly to the LHC, but they are accelerated gradually. It takes approximately 20 minutes to accelerate the particle to the final energy. Procedure of accelerating:

- protons are extracted from a hydrogen atom by an electric field
- *Linac 2* - linear accelerator, up to energy 50 MeV
- PSB (*Proton Synchotron Booster*) - circular accelerator, up to energy 1.4 GeV
- PS (*Proton Synchotron*) - circular accelerator, energy 25 GeV
- SPS (*Super Proton Synchotron*)- circular accelerator, energy 450 GeV
- LHC

The collisions in LHC are detected in 4 experiments: ALICE, ATLAS, LHCb and CMS. The scheme of accelerating is shown in the figure 1.1.

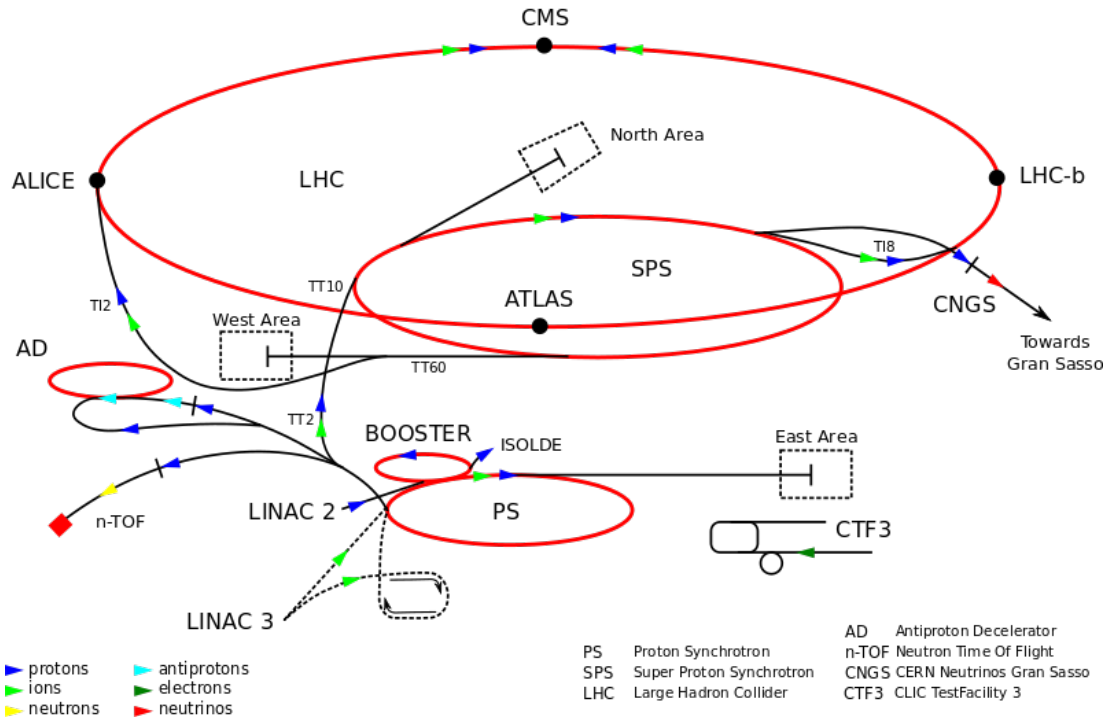

Figure 1.1: Procedure of accelerating [3]

1.2 ATLAS

In this section ATLAS (*A Toroidal LHC ApparatuS*) detector will be described. ATLAS has got according to [4] cylinder shape, it is 46 meters long and its diameter is 25 meters. The figure 1.2 shows ATLAS detector.

ATLAS detector is divided to many subsystems. Every subsystem (which is called subdetector) is designed to give different information about the particles. The subdetectors are:

- Inner detector
- Electromagnetic calorimeter
- Hadron calorimeter
- Muon spectrometer

The Inner detector (ID) is the subdetector closest to the collision. Its function is to measure track of a particle and determine its momentum by measuring its bending in a magnetic field. ID contains of 3 types of detectors: silicon pixel detectors, silicon strip detectors (which are called Semiconductor Tracker (SCT)) and Transition Radiation Tracker (TRT). The principle of the silicon detectors will be described later. The pixels are small rectangles with size 50x300 μm and strips are small 12 cm long stripes which are distanced 80 μm. TRT consists of a metal tubes with diameter 4 mm surrounded by a material which creates transition radiation [5]. The track of the particle can be reconstructed by the signals in each pixel/strip/TRT. Every part of the Inner Detector consists of a few coaxial barrels which are closed by discs on the both sides. This is shown in the figure 1.2.

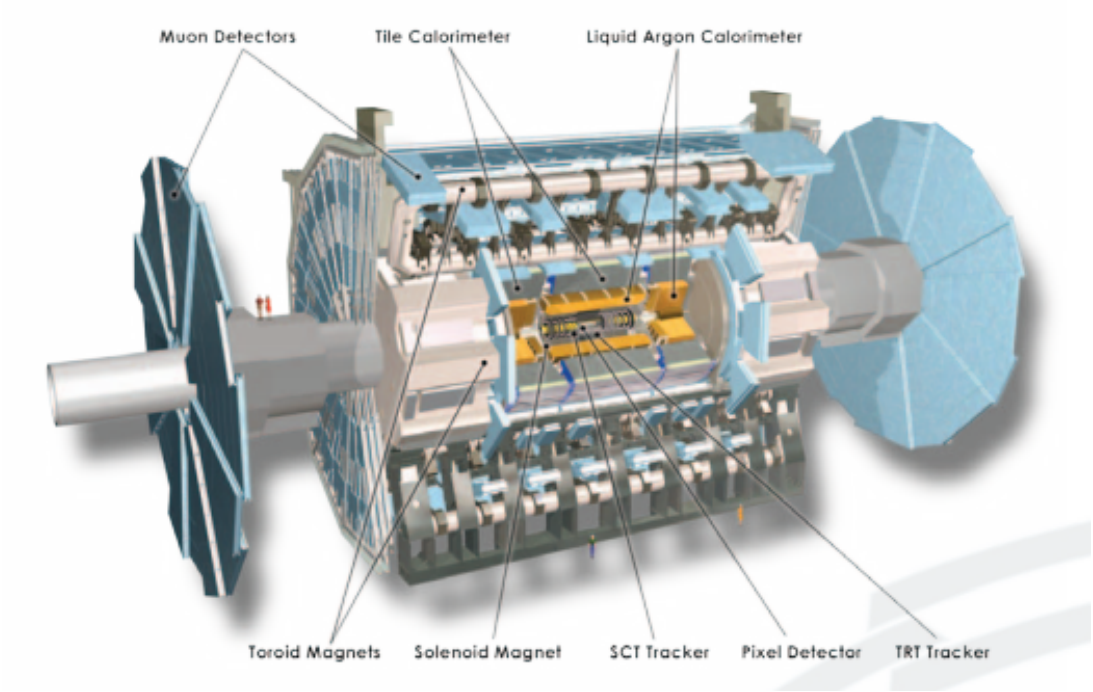

Figure 1.2: Detector ATLAS [4]

The calorimeters are detectors designed to absorb the particle and determine its energy. The function of the calorimeter is to slow the particle in matter and to create a particle shower (electromagnetic or hadron). The sum of energy of created particles from the shower is equal to the energy of the original particle. In calorimeters there are two environments: an absorber (metal plate) which absorbs particle and creates the particle shower and sensing element which detects the particles from the shower.

In ATLAS there are two kinds of calorimeters - electromagnetic and hadron. Electromagnetic calorimeter absorbs electrons and photons; hadron calorimeter absorbs protons, neutrons, pions and other heavy particles.

The purpose of the muon spectrometer is according to [6] to detect muons. Because they are 200-times heavier than electrons they do not create large particle showers in the calorimeters. In the spectrometer there is a large magnetic field which is used to measure momentum of the muon. Muon spectrometer has got two types of detectors:

- Monitored Drift Tubes - an aluminium tubes filled with special gas. Muon interacts with gas an along its path creates ions. Ions drift to the electrodes where the signal is detected.
- Cathode Strip Chambers - proportional chambers with cathode segmented to the strips. This chamber is unlike drift tubes able to operate in environment with high particle density (near beam pipe).

1.3 ATLAS Upgrade

Currently the upgrade of detector ATLAS is being prepared. ATLAS Upgrade is according to [7] planned to be initiated in 2025. The detector must be prepared

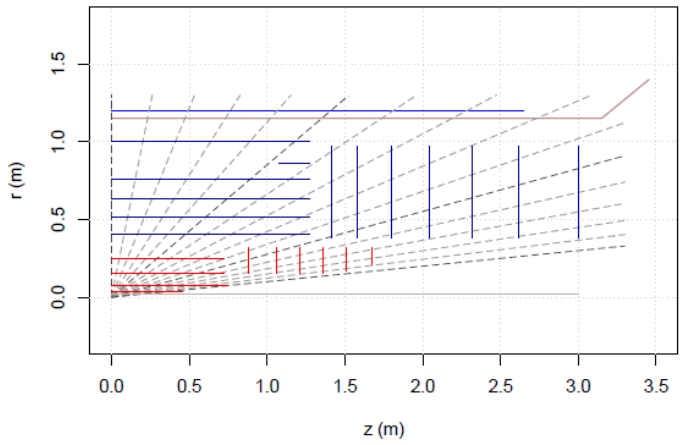

Figure 1.3: Layout for pixel and strip detectors [7]. Red lines represent pixel and blue lines strip layers, horizontal lines represent barrels and vertical end-caps. In (0,0) is the position of collision

to handle a large amount of luminosity given by HL-LHC (*High Luminosity LHC*) which means that the parts of detector must be upgraded for this amount of radiation. Higher luminosity will open a new area of searching for the new physics and will widen the possibilities for the study of the characteristics of the Higgs boson. The luminosity will start in 2025 with $5{\cdot}10^{34}$ $\mathrm{cm}^{-2}\mathrm{s}^{-1}$ and during 10 years will increase to integrated luminosity of 2500 fb^{-1}. HL-LHC will again collide proton with proton.

1.3.1 Inner detector - ITK

The upgrade of detector ATLAS will affect all the subdetectors - detector as well as electronic parts. But the main focus will be only on the inner detector's semiconductor strip detectors which is the focus of this thesis. At first, the inner detector will be given new name: *Inner Tracking System* (ITK). The current inner detector is not capable of operating in such high radiation as planned. That means that it will have to be replaced. The new inner detector must be designed to resist and to be able operate in a higher radiation and in an environment with a large multiplicity of the collisions (the number of the interactions in one proton collision will increase from 23 to 200).

Currently the technology for the upgrade is being prepared and the prototypes of detectors are being produced and tested.

The biggest change in the inner detector will be use of solely silicon parts - no transition radiation tubes. TRT will be replaced with an additional semiconductor long strip layers. ITK will be again divided into barrels and end-caps. Barrel will consist of 4 pixel, 3 short and 2 long strips layers and end-cap of 6 pixel and 7 strip discs. Between barrel and end-cap strips there will be small stub barrel to cover space between them. The length of strips will be 23.820 and 47.755 mm. The final layout has not been decided yet, but in the figure 1.3 one possible is shown.

The strip silicon detectors will be placed in ATLAS detector in bigger pieces

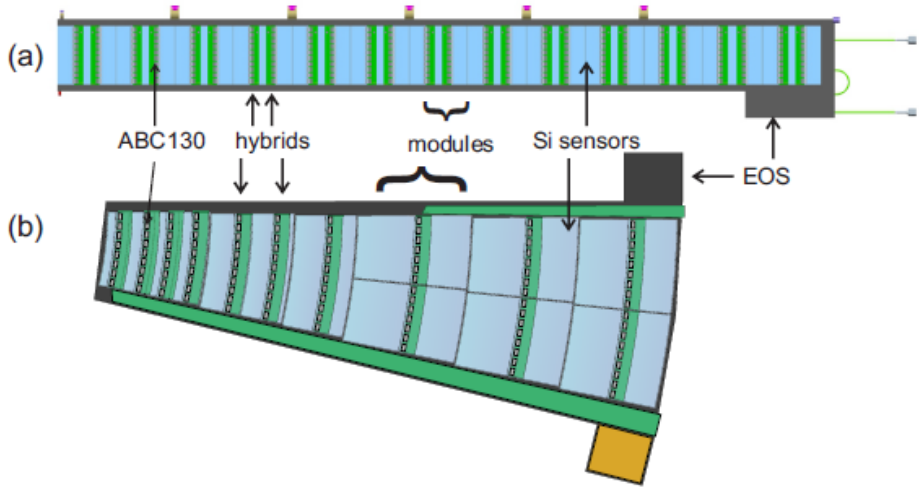

Figure 1.4: Layout of modules in stave (a) and petal (b) [7]

which are called staves and petals. Each of them will consist of modules. Modules are units consisting of the silicon detector and electronics. The stave is a building unit of a barrel and the petal of an end-cap disc. Their schemes are shown in the figure 1.4.

The stave and petal will be the cores that provide mechanical strength, support for module, electrical, optical and cooling function. Stave will be placed into circle and will be tilted by 10° and overlapped. This arrangement is shown in the figure 1.5. The petals will be used to create discs. For the creation of one disc 32 petals will be needed. The petal will consist of 9 modules which create 6 circles. The outer three circles will have each two modules; the inner two circles will have each one module. This can be seen in the figure 1.4b). The arrangement of petals into disc has not been decided yet. The two possibilities are turbofan and castellated layout and are shown in the figure 1.6.

The strips on the modules for the stave are parallel with the sides of the detector. For the petal strips they are radial and aim to the beam which allows to measure $r\phi$ coordinate.

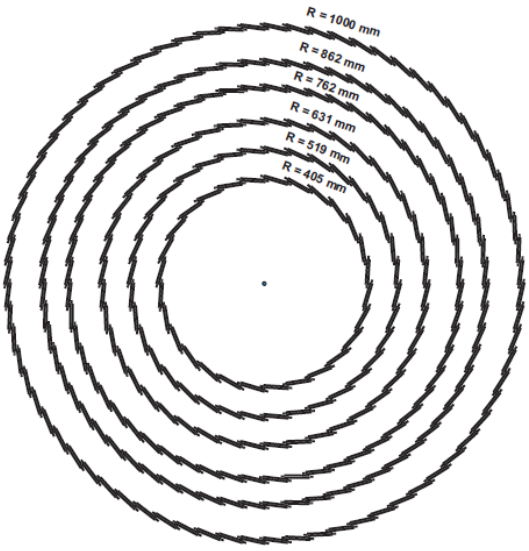

Figure 1.5: Arrangement of the stave - tilted by 10° and ovelapped [7]

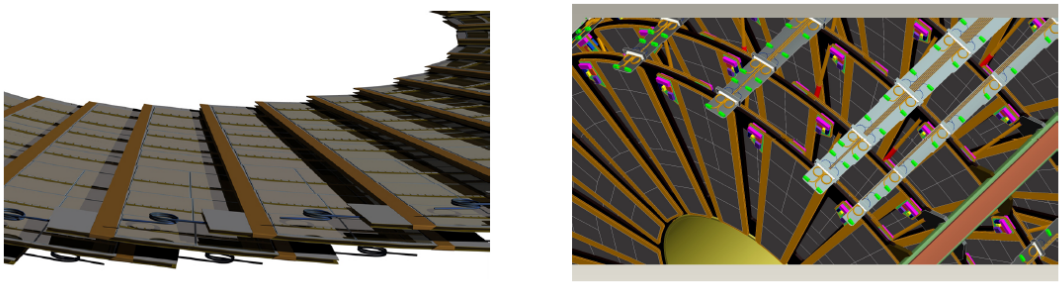

Figure 1.6: Two possible arrangements of petals into disc: turbofan (left) and castellated layout (right) [7]

2. Strip silicon detectors

In this chapter the principle of the strip silicon detectors will be described.

At first there will be explained semiconductors, generation and transport of carriers in them. Then there will be description of PN junction as the most simple semiconductor detector and finally the strip silicon detectors. The information used in this chapter is according to [8], [9], [10].

2.1 Semiconductors

Semiconductors are elements of IV.A group in the periodic table. In the lattice they are arranged so that each atom shares its four valence electrons with the neighbouring atoms.

Their typical properties result from the band structure which can be seen in the figure 2.1 - almost full valence band is separated from the conduction band as for insulators but the gap is much smaller for semiconductors. The gap is only 1-3 eV wide and it can be overcome by thermal motion.

At low temperatures the valence electrons remain bonded (in the valence band). But at the higher temperatures thermal vibrations might cause the valence electron to overcome the gap between valence and conduction band and to become a free electron. The free electron leaves behind a free place: a hole. The formed hole can be filled with another electron from the valence band meaning the hole can move inside the semiconductor.

The most commonly used semiconductors in detector physics are silicon and germanium - in this thesis only the silicon detectors will be used.

Semiconductors are divided into intrinsic and extrinsic semiconductors. The intrinsic semiconductors contain no impurities; they contain only one kind of atoms.

Since it is extremely difficult to obtain such purity for an intrinsic semiconductor they are used very rarely. Instead, the extrinsic semiconductors are used by purposely adding atoms of a different element. Depending on the type of admixture used, the extrinsic semiconductors are divided into n or p-type. If the added atoms have got excess electrons (donors) the semiconductor is n-type. If

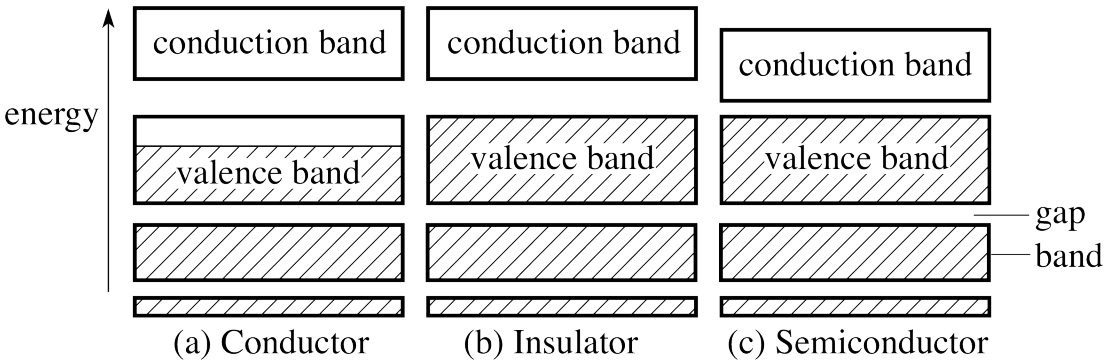

Figure 2.1: The band structure of conductors (a), insulators (b) and semiconductors (c) [11]

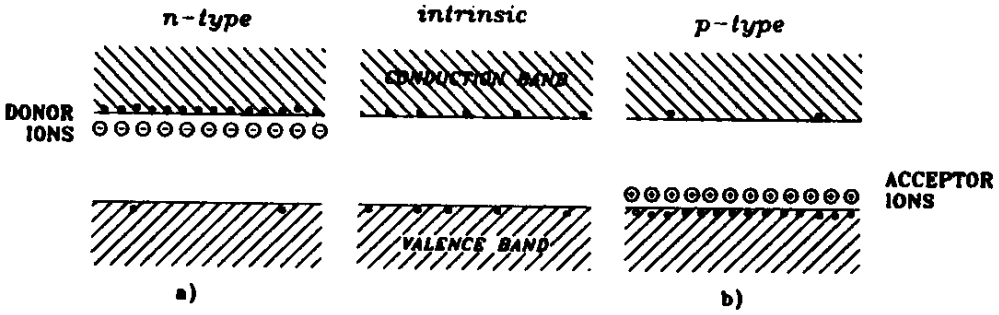

Figure 2.2: The band structure of intrinsic and extrinsic semiconductors [10]

the added atoms have got lack of electrons (acceptors) it is p-type semiconductor. If the doping of the admixtures is large they are called n^+ or p^+. If the ratio of donors and acceptors in semiconductor is approximately the same it is called compensated semiconductor.

In the band structure adding of donors or acceptors causes the creation of localized energy levels in the band gap between valence and conduction band, see the figure 2.2.

2.1.1 Carrier transport in semiconductor

A transport of carriers in semiconductor is provided by non-uniformity or external electric or magnetic field.

If the electric field is present, it will cause movement of the electrons and holes and their acceleration depends on the field intensity. The direction of the movement is determined by the external electric field. This movement is called drift.

In a field-free case, if the charge in semiconductor is unevenly distributed, particles start to diffuse. Diffusion is movement of charge from the place with higher concentration of charge to the place with lower concentration.

If the external magnetic field is present, the transport of carriers is affected by the Hall effect. In magnetic field, the Lorentz force affects moving charged particle which results in deviation of particle from the origin direction. Thereby the current in semiconductor will decrease and the electric field perpendicular to movement direction of the particle will appear.

2.1.2 Generation of carriers

As mentioned before, the carriers are generated by lifting electrons from valence into conduction band and leaving a hole behind. Mean energy of creation of one electron-hole pair (e-h pair) is 3.6 eV. This energy can be gained by various mechanisms, such as thermal agitation, optical excitation or ionisation by penetration of charged particles.

Thermal generation of the electron-hole pairs causes undesirable effect in the detectors because it leads to noise overlapping the measured signals. In some semiconductors, the gap between valence and conduction band is so small that

thermal generation occurs at room temperature. That means that those semiconductors (e.g. germanium) have to be cooled to lower temperature or the other semiconductor with wider gap have to be used. Silicon generates a low noise in room temperature.

The generation by electromagnetic radiation (optical excitation) is the basis of photo detectors. An electron absorbs a photon and its energy is used to lift the electron to one of the states in the conduction band (only if the photon energy is higher than the gap). The electron and hole will subsequently move towards the band-gap edges which results in emitting the energy in the form of photon.

When a particle goes through the material it ionizes and leaves behind (creates) a lot of electron-hole pairs along its track. Depending on the type of particle, the generation of the charge cloud may include rather complicated processes. The semiconductor detectors are suited for the particles:

- *Visible and ultraviolet light* - one e-h pair is usually generated.
- *X-rays* - the number generated e-h pairs depends on the energy and the spatial region is small.
- α *particles* - their ionisation is strongly velocity dependent. It is described by Bethe-Bloch formula. Density of e-h pairs increases with the path length.
- β *radiation (electrons)* - electrons ionize less than α. β radiation penetrates deeply into semiconductor, producing constant e-h density along its path and it remains relativistic.
- *High energy charged particles* - the energy is so high that the energy loss through material is negligible. The density of e-h pairs is constant along the path length. A single relativistic charged particle is called minimum ionizing particle (MIP).
- *Non-relativistic charged particles, e.g. protons or nuclei* - ionisation is dependent on inverse particle's energy and square of charge. This can be used to measure ionisation and identification of particle.

Other types of radiation (neutrons, high energy photons) can create electron-hole pair, but the probability of doing so is small. That is why semiconductor detectors are not suitable for detecting these kinds of particles.

2.2 Semiconductor detectors

2.2.1 PN junction

The simplest type of semiconductor detector is PN junction. It is created by combining p-type and n-type semiconductor. This electric component can be put in electric circuit in forward or reverse direction. Only one direction of insertion into circuit (forward) conducts current.

In the reverse direction electrons diffuse to p region, the holes to n. The region around the junction is empty (depleted) with no charge carriers and on the edges

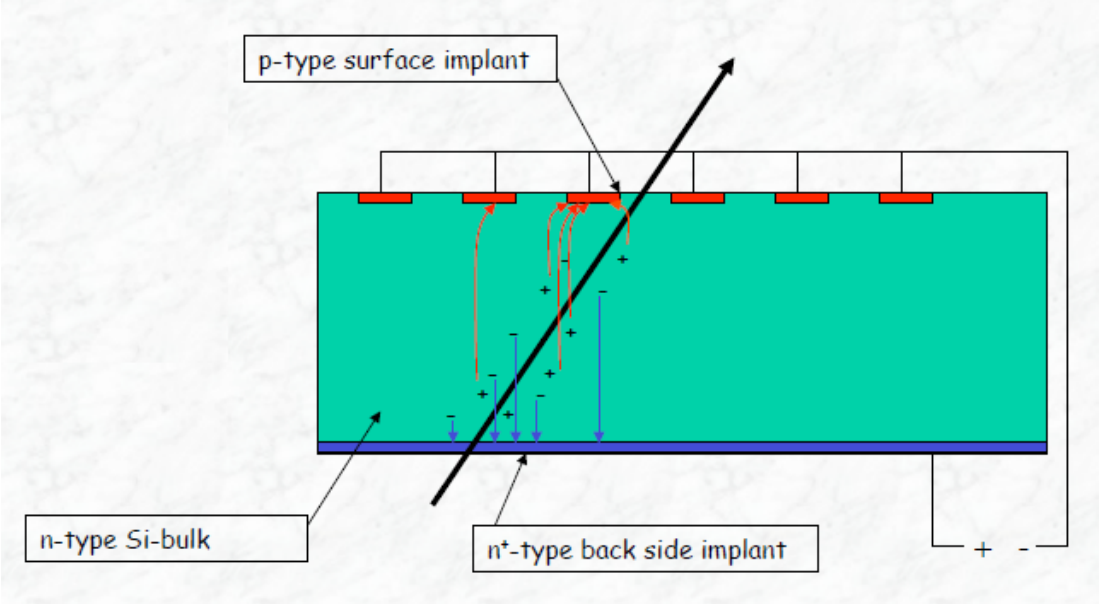

Figure 2.3: Scheme of detection in semiconductor detector [12]

there is positive and negative charge, which creates potential V_i. The depleted region is called a space-charge region.

For detection the larger space-charge region the better, which means the V_i has to be as big as possible. That is why the external voltage V_{ext} is used.

Even in the fully depleted junction the charge carriers can be created (e.g. from thermal excitation). Creation of the carriers results in presence of reverse-bias current. At some point the bias voltage is so high that the breakdown occurs and the reverse-bias current increases drastically with higher voltage.

2.2.2 The principle of semiconductor detectors

The most important part in a semiconductor detector is depleted PN junction. Usually the edges of PN junction are made of p^+ and n^+-type semiconductor.

The scheme of a semiconductor detector is shown in the figure 2.3. A particle flies through space-charge region and creates electron-hole pairs along its path. Pairs drift to the poles due to the electric field - electrons to positive and holes to negative pole. Drifted electrons in p-part create an electric signal which is detected.

2.2.3 Strip semiconductor detectors

If the p-type part of semiconductor is not divided (in one block), it cannot be said where exactly the particle was detected. That is why it is needed to divide p-part into smaller parts. Usually the division is into small rectangles or stripes. The detectors with small rectangles are called pixel detectors and with the stripes, strip detectors. In the current ATLAS detector the size of pixel detector is 50 x 300 μm^2. The strip is 18 μm wide and the distance between two strips (pitch) is 80 μm.

One pixel detector provides an information about both x and y directions and one strip detector provides only one of the direction. That is why they are used

double-sided, the second is rotated (in ATLAS the rotation is 40 mrad). The size is usually limited by the detection electronics. The electronics is mandatory for readout for every semiconductor detector. The information about z direction is gained from placement in the detector system.

2.3 Detector signal

The signal readout from detector can be digital (binary) or analog. In the analog readout an information about amplitude is given. In the binary readout the result is only 1 or 0: 1 if the signal is higher than set threshold and 0 if the signal is smaller. In ATLAS detector the binary readout is used.

From binary readout one cannot get the amplitude from one signal, but can get a distribution of amplitude from many signals. This can be obtained from a threshold scan, where the threshold is increased and the number of injected calibration pulses with constant amplitude that reads as 1 is counted. The result of such measurement is step function or in case the noise is present it is error function. They are integral distributions - integral of the signal without noise which is delta-function is a step function. And integral of the signal with noise which is Gaussian distribution is an error function. These distributions are shown in the figure 2.4.

From the threshold scan the information about noise can also be obtained, if the result of threshold scan is fitted by error function. Error function is special function of sigmoid shape [13]. In our case the complementary error function is used, because it starts at y = 1 (not -1 as original error function). The definition of complementary error function is:

$$\begin{aligned} \mathrm{erfc}(x) &= 1 - \mathrm{erf}(x) \\ &= 1 - \frac{2}{\sqrt{\pi}} \int_0^x \mathrm{d}t \; e^{-t^2} \\ &= \frac{2}{\sqrt{\pi}} \int_x^\infty \mathrm{d}t \; e^{-t^2} \end{aligned} \tag{2.1}$$

Three parameters are fitted in the result of threshold scan: constant, σ and vt50. The fitted parameter σ is the noise, vt50 is 50% point (mean) - point with the highest slope and the constant describes a number of injected pulses. The fitted function is:

$$\mathrm{erfc}(x) = \frac{C}{2}\left(1 + \mathrm{erf}\left(\frac{vt50 - x}{\pi\sigma}\right)\right) \tag{2.2}$$

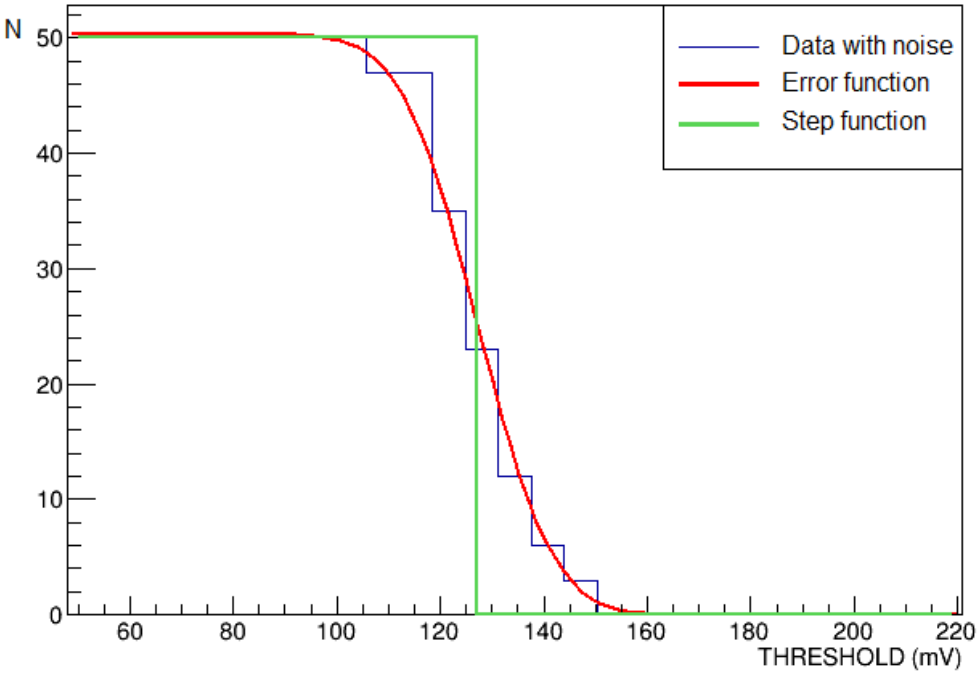

Figure 2.4: Result of threshold scan

3. Tests with modules

The construction of every part of module is a long process, because every single part has to satisfy criteria for quality and service life. That means that every part is tested before and after module construction.

This thesis focuses only on ATLAS Upgrade. Since the status on the upgrade is that the prototypes are being made, currently only the prototypes are being tested. Specifically in this thesis, two prototypes of the silicon semiconductor detectors will be tested - one module from Freiburg and the other from Zeuthen, both sensors from Barcelona.

3.1 Motivation

The purpose of the semiconductor detectors used in SCT and later in ITK is to measure track of a particle with the lowest error possible. From the position of a particle and with the use of the magnetic field the momentum is calculated. The momentum and its uncertainty are important for the analysis.

During development of the new silicon detectors a prototype is made. The prototype's performance has to be tested to continue the research.

3.2 Individual tests

In this section the different tests will be described: electric tests, test beam, tests with radioactive source and laser tests [14]. Every kind of test has its pros and cons.

Electric tests are series of tests during which the module generates and inserts a calibration pulse from its electronic circuit and then it reads out the signal. For these kinds of tests it is not necessary to have an external source.

Test beam, tests with radioactive source and laser tests are tests with an external source. The idea is to imitate MIP and to see the response of the module. These tests are only used during prototype development.

The test beam is the best type of test regarding to imitating the MIP, because the real beam is used. It gives information about particle position because the detector is placed between telescopes (position-sensitive detectors). The cons are the price and rather complicated organisation of the event.

Detector testing with radioactive beta source is on the one hand cheap and the absolute value of the signal of the real particle is measured. On the other hand there is no information about position, because if telescopes are used, the particle will not go through all layers until the end where triggering scintillator is located. With these tests the deposited energy of particle can be obtained.

The laser test is moderately expensive (depending on the price of the special equipment) but it gives precise information about the position because the laser can be focused. When using laser, many pulses can be created which results in a good statistics. Unfortunately there are present some optical effects and the δ-electrons are not created which means that the cluster size [1] is much smaller

[1] The cluster size is number of strips with a response under some conditions.

than in the MIP. Optical effects include reflection and refraction of the light on the surface (especially on the strip) and other layers. Laser test also gives only relative information about the signal, because the amplitude of laser can be adjusted.

For the laser tests usually there are 2 lasers used: red and infra-red. Infra-red laser penetrates deeper into silicon, but it can reflect on the lower detector layer causing non-desired optical effects. Red laser penetrates only the surface which is good because no addition reflection happens but it does not cover the whole detector area. Generally red laser gives information mainly about electronics and infra-red laser about the sensor.

After prototype development, modules are manufactured. Before installing in the detector, series of thorough tests are done. For ATLAS it contained mechanical inspection, temperature test, basic module characteristics and IV characteristics. These tests will be also done (but modified) for the ATLAS Upgrade. During the run of detector ATLAS the electric tests are also done.

In this thesis only the electronic and laser tests were done.

3.3 Testing laboratories

Tests were done at first in an electronic lab, later the laser tests in a clean room. Both labs are situated in IPNP (Institute for Particle and Nuclear Physics) in Prague.

The electronic laboratory serves for development, manufacturing, testing and diagnostic of electronics [15]. The photo of the lab is shown in the figure 3.1.

The clean room is special room where the air is filtrated, without dust and the room has monitored constant temperature and humidity. Before entering the clean room it is needed to take off shoes and wear a special lab coat. In the figure 3.2 is the photo of clean room where the most of the tests were done, especially all the laser tests. The clean room is suitable for testing modules because the dust will not cover it (if the detector is covered with dust it can change its detecting properties). Also, constant humidity prevents the condensation of moisture on a sensor.

3.4 Equipment for testing

For testing of a module one needs to have proper equipment - mainly power supplies to power up the chips and the module itself and also some system that reads the signal from the chips.

HSIO is abbreviation of *High Speed Input Output*. It is a board which is used for reading out the detector and communication with a computer. It is shown in the figure 3.3. The software for the HSIO is called SCTDAQ. It is ROOT-based program [16] which communicates with module and also has pre-programmed tests - few of them will be mentioned later.

When turning on and off the whole apparatus, a particular sequence has to be followed. When powering up:

1. Vacuum pump - it pulls the detector closer to the surface - cooling is much more effective and the detector will not move during tests.

Figure 3.1: The photo of the electronic lab in IPNP [15]

Figure 3.2: The photo of the clean room in IPNP

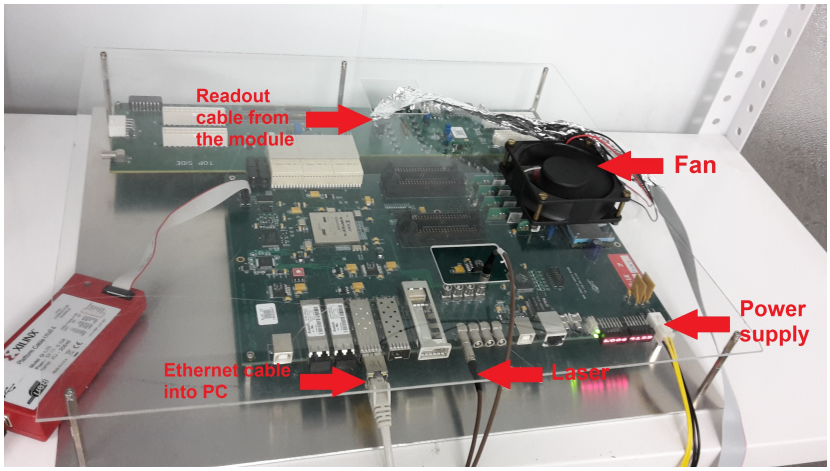

Figure 3.3: The photo of HSIO with marked components

(a) vacuum pump

(b) cooler

(c) power supplies; from the left: high voltage, two low voltages and HSIO power supply

Figure 3.4: The photos of vacuum pump, cooler and power supplies for HSIO, low voltage and high voltage

2. Cooling - detector needs to be cooled so the higher voltage can be used during measurements and the reverse-bias does not create breakdown.

3. HSIO voltage - it has to be powered to function properly with voltage 48 V and current 0.5 A.

4. Low voltage - it is used to power up the readout chips in detector. It is needed to have two sources. For the module from Freiburg the source was 4.5 V/0,32 A and 2.7 V/1.55 A and for the module from Zeuthen 5 V/1.43 A and 2.99 V/2 A.

5. High voltage (if needed for the particular test) - it is used to deplete the detector so it can function properly (preferable the voltage is higher than full depletion voltage). The bias voltage has to be negative.

All these components are shown in the figure 3.4. When detector and reading hardware is powered on, readout software (SCTDAQ) can be run. Of course, SCTDAQ can be launched without detector and HSIO powered up, but no signal will be read. When turning off, the procedure is reversed.

For the laser tests, more equipment is needed:

- Laser - for the laser tests the 2 lasers were available: red (660 nm) and infra-red (1060 nm). The laser is located above module and points into strips.

- Pulse generator - to create a pulse for laser which illuminates module.

- Oscilloscope - this component is not necessary, but is used to see the shape of the pulse.

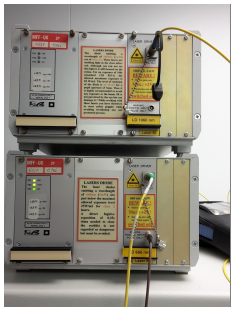

(a) red (down) and infra-red (up) laser

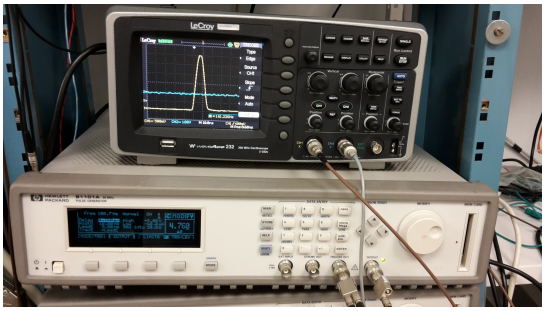

(b) pulse generator (down) and oscilloscope (up)

Figure 3.5: Photos of pulse generator, oscilloscope and lasers

- Motion stages - it is a device which can be automatically controlled. It is not necessary either, but without it no automatic laser test can be done.

The photos of these components are shown in the figure 3.5.

3.5 Modules and their layout

For the testing two modules were available: one from Freiburg and one from Zeuthen, both sensors are from Barcelona. The first tests were done on Freiburg module (in that time it was the only one available), later on Zeuthen module. In the figures 3.6 and 3.7 there are photos of the detectors.

Both sensors are end-cap strip silicon detectors which means that the strips have a radial shape. The strip size is around 20-30 μm and the distance between two strips (pitch) is around 80 μm. Both sensors are composed of 2 rows of sensors which are called Stream 0 and 1. Both streams of both modules have got 768 strips.

In a lab the module is placed in thermally isolated test chamber (black box [15]) which has to be closed during measurement because the detector is light sensitive - with light present the leakage current raises. In the figure 3.6 is shown the layout of the test in the black box. The module is laid on the cooled base (connection of the cooling pipe is not visible in the photo because it is in the back) where it is sucked in by the vacuum. On the right side it is connected by cards to the high and low voltage (two power supplies for low voltage and one for high voltage). On the left side the readout cable, which transfers information into HSIO, is located.

In the figure 3.3 the layout of HSIO is shown. There can be seen the readout cable which is connected to the module, Ethernet cable which communicates with PC and the cable which provides power supply. The cable which connects HSIO with pulse shaper (only for laser tests) can also be seen. Pulse shaper is connected to the laser.

The layout for the laser test can be seen in the figure 3.7. The laser is located above the module and points onto the strips. It emits pulses when the signal comes from the pulse generator. The laser is attached to the motion stages, which can be controlled remotely from PC. The 3-axis laser positioning stages (Standa) with step 0.2 μm in 3D and 2 rotations is used [15]. Motion stages were

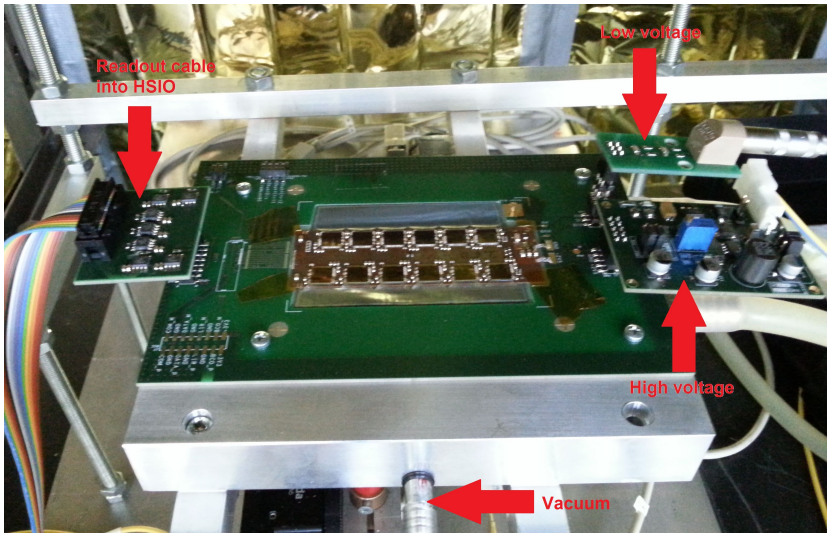

Figure 3.6: The photo of module from Freiburg with power supplying, readout and vacuum components

not available from the beginning, but thanks to Martin Sýkora's bachelor thesis [17] it was made fully functional and operational remotely from PC.

The scheme of whole layout is shown in the figure 3.8.

When measuring without an external source, the detector has to use internal trigger. The system described above works as follows. While measuring, for example, a threshold scan, SCTDAQ sends information into HSIO. HSIO tells the module to insert a calibration pulse and then to readout this signal. Note: timing between inserting a calibration pulse and readout have to be set up using the particular test.

The communication of the system with laser works differently. When, for example, the threshold scan is being measured, SCTDAQ tells HSIO that it wants to readout data. HSIO sends out signal into pulse generator which sends out signal about shape of pulse for the laser. Photons from laser interact with detector and create e-h pairs. The pairs drift into electrode where their signal is readout. It the timing between laser pulse and readout is right, the whole signal is readout. If the timing of readout is off, none or just the part of the signal is read.

3.6 Threshold scan

In this section the threshold scan in SCTDAQ will be described, because this test will be used later. The principle of threshold scan was described in section 2.3.

In SCTDAQ the test which does a single threshold scan is called ABCN scan. Before running the scan, range of threshold (in mV) and threshold step can be entered. If not, a default values are used. ABCN scan runs threshold scan on each strip separately and then the data are fitted with error function. The data and results are saved in .root file.

Note: when the external source is not used, the result is noise. When the source is used, the information about signal is obtained.

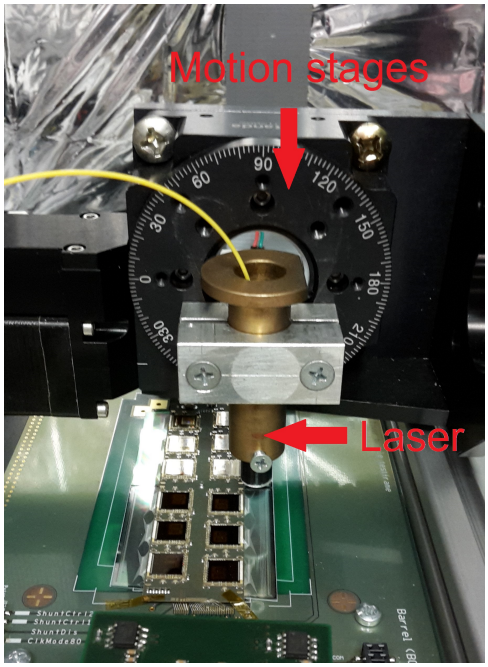

Figure 3.7: The photo of module from Zeuthen with laser and motion stages

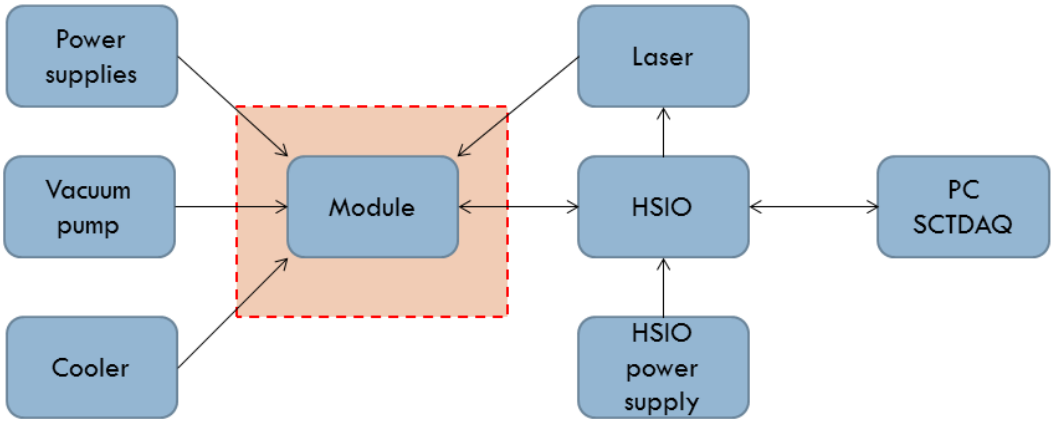

Figure 3.8: The scheme of layout for the tests, red dashed line shows the black box and the arrows show the communication between the components

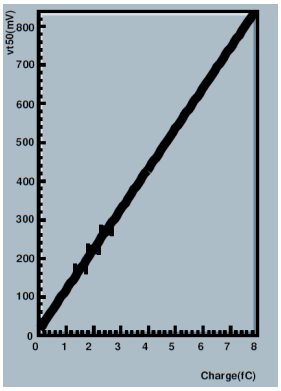

Figure 3.9: Result of the Three Point Gain - three points fitted linearly

3.7 Three Point Gain

Three Point Gain (3PG) is one of the tests SCTDAQ provides. It is based on the threshold scan. 3PG provides a calibration between collected charge and internal threshold units (mV). During this test HSIO injects into every strip 3 charges (1.5, 2 and 2.5 fC) and does a threshold scan. The result is graph, where in x axis is injected charge and in y axis is vt50. There are 3 points (for every strip) which are fitted with a straight line. Example of the graph is shown in figure 3.9. From the fit SCTDAQ gets gain and noise as:

$$vt50[\text{mV}] = gain[\text{mV.fC}^{-1}] \times charge[\text{fC}] + offset[\text{mV}] \tag{3.1}$$

where offset gives information about pedestal. Pedestal consists of noise and electronic offset. The electronic offset can be set to artificially raise a pedestal.

The linear dependence is not exact, because if the number of injected charges and their values would be higher, result will be a polynomial. In SCTDAQ there exists this kind of measurement called Response Curve, which inject 10 charges and the result curve is fitted polynomially. It gives more precise information about offset and gain. In this thesis only 3PG was measured since the Response Curve did not work in SCTDAQ.

3PG is used to measure the noise of a detector as a function of bias, temperature, etc. The higher the bias voltage is, the lower the noise should be. When the full depletion bias voltage is reached, noise does not change - it stays constant. For the higher temperature the noise should be higher than for lower temperature because of thermal excitations.

The results (offset and gain) from 3PG will be later used to convert measured vt50 into charge using equation 3.1.

3PG was done on both modules for different temperatures and pedestals (raised artificially using trim file, will be explained later). At first, the dependence of measured noise (not raised by trim file) and bias voltage was measured. The results can be seen in the figures 3.10 for Freiburg module and 3.11 for Zeuthen module. For both measurements the temperature was 15°C. On y axis there is average noise for the whole module since the 3PG insert charge and evaluates noise for every channel in the module. The variable used in y axis is Equivalent Noise Charge (ENC) measured in electrons e^-. It is the result of dividing the measured noise by the gain and converting fC to electrons (1 fC = 6250 e^-) [18].

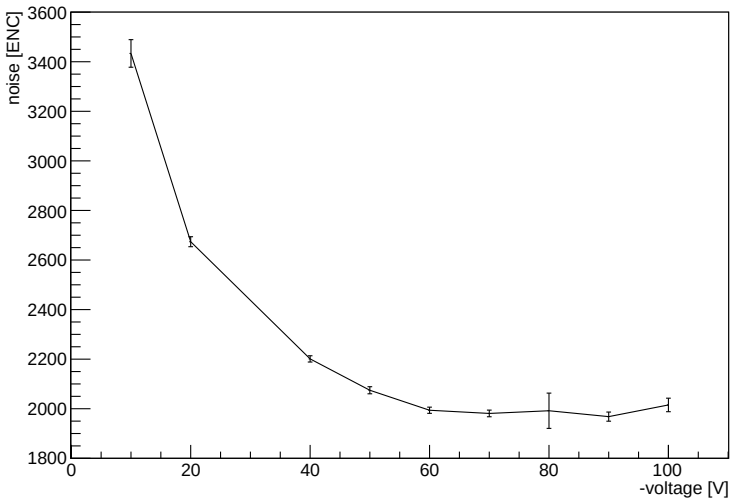

Figure 3.10: Noise vs. bias voltage for module from Freiburg

In the graphs one can see that the noise dependence is the one expected - with higher bias voltage the noise is lower. The Freiburg module has got a very high noise which means that this module does not satisfy the requirements. The Zeuthen module is in this consideration a better module.

The leakage current has an impact on the maximum bias voltage that can be set on the module. Leakage current in Freiburg module is higher than for the Zeuthen module, which means that the noise is higher for Freigurg module. The result is that the maximum bias voltage for Freiburg module is -100 V with current -28 μA and for Zeuthen it is -130 V with current -20 μA. Both voltage and current are negative; from now on they will be mentioned as the absolute values.

The noise trend in Zeuthen module is decreasing but it looks like it is not saturated. This can be caused by not reaching the full depletion voltage. But in this case, the voltage could not be raised because of high leakage current (which should not be higher than 20 μA).

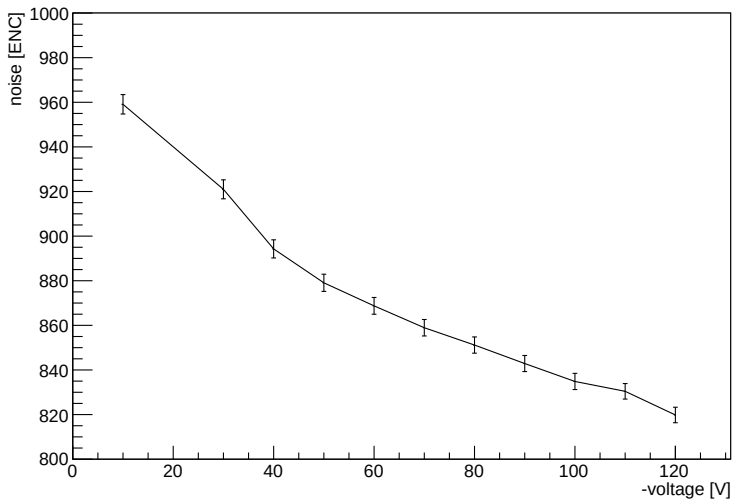

Figure 3.11: Noise vs. bias voltage for module from Zeuthen

4. Laser Tests

In this chapter all the measurements and the results from the laser tests will be described and shown. The order of test descriptions will be the same as the order of the measurements. That means that at first the module from Freiburg will be tested and later the module from Zeuthen.

All graphs were created in the C-based program ROOT. The names of axes for the motion stages are used as followed:

- x axis - axis which is along the strip
- y axis - axis which is perpendicular to the strips
- z axis - axis which describes distance between the module and laser

All tests that were done are threshold scans. The response was measured as a dependence of a position of laser or timing, which they will be called y/z-position scan and timing scan. Note: a timing scan is both change of timing and y-position of laser.

4.1 Module from Freiburg

Only the laser tests with red laser were done on this module .

4.1.1 Red laser

Manual laser movement

The very first test with laser was y-position scan with a manual movement of the motion stages. Manual movement means that the measurement was not done automatically, but the laser was controlled electronically by computer program where the axis and the shift had to be inserted manually.

The test was done for voltages 80 V and 30 V and temperature 15°C. For both voltages 40 y-position scans were measured with step of 10 μm. The result graphs, vt50 vs. laser position, are in the figure 4.1.

In these graphs one can see that the laser is not focused enough to see a reflection of laser on the strip. That means that to continue measurements, the laser had to be focused. In the graphs can be also seen that the strips are not in order. It means that this module has got a bad bonding, which means that electronics which recognises a strip as, for example, 251 is not connected via bond to the strip 251, but to some other strip.

For measurement of the best focused z position of laser the automatic scan with a laser movement had to be created. It could have been done without it, but it would take a very long time to measure. At this point two macros for measurement were created - one for a position scan in one axis movement and the other with two axes movement, which will be called 2D threshold scan.

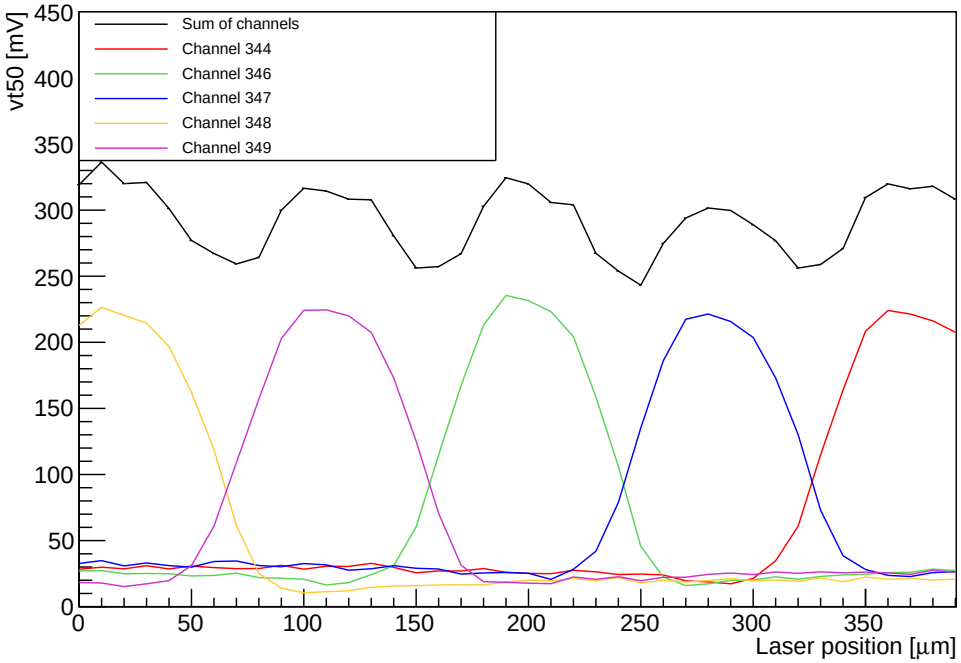

(a) 30 V

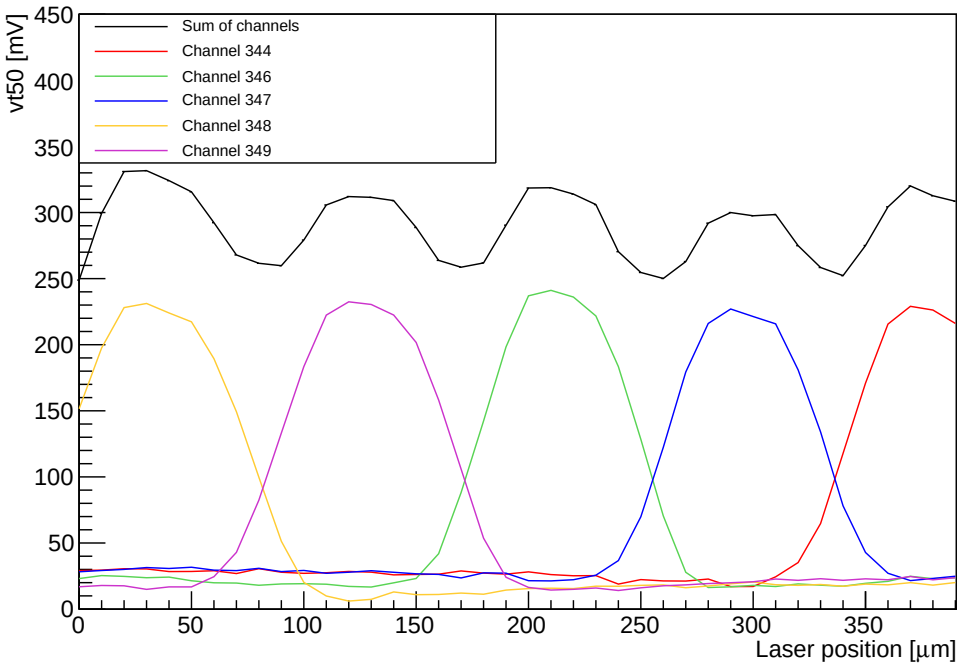

(b) 80 V

Figure 4.1: y-position scan with manual movement, laser step of 10 μm

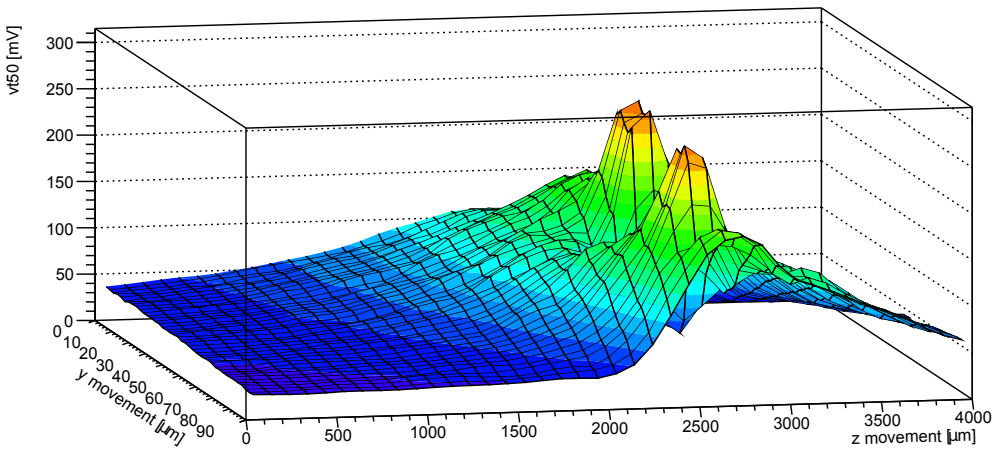

Figure 4.2: Focusing of the laser, the best position is for $z = 2.6$ mm

Laser focus

With 2D threshold scan (y and z axes movements) the focus of the laser was measured. The range in y axis was 0-90 μm with step of 2 μm and in z axis 0-4 mm with step of 0.2 mm. The temperature during measurement was 15°C and bias voltage was 80 V. The result is shown in the figure 4.2. From this 3D graph can be seen that one z position stands out, where the laser is focused and the reflection on strip can be seen. It is for $z = 2.6$ mm.

After evaluation of the laser focus, the next same 2D threshold scan was measured to make sure the laser was moved to the focused position. For z axis it was only for 3 positions, +50 μm, 0 μm and -50 μm, where 0 μm is the focused position from the previous measurement. The result of focus check is in the figure 4.3. It can be seen that the 0 μm position is good, because it has got the highest slope. Note: the minima are not in the same position because laser is not exactly perpendicular to the module.

Fine interstrip scan

When the laser is focused, the next step is to measure y-position scan with a finer step. This was done using the macro that was written (and the all next measurements were done using one of these special macros). The laser position range was 0-400 μm with step of 0.5 μm, temperature 15°C and bias voltage 80 V. The result can be seen in the figure 4.4, one graph with y axis vt50 and the other with charge.

For this measurement it was for the first time (since it was not necessary for the previous ones) subtracted pedestal and converted mV into fC using the equation 3.1 and the result of 3PG for the same thermal and voltage conditions.

In the graphs there can be finally seen the reflection on the strip and the behaviour is as expected: nothing collected when the laser points exactly into the strip and something collected everywhere else.

The channel 347 has got lower response.

In the middle of two strips there is some major signal loss. This could be caused by many reasons: the timing between the laser pulse and readout in not

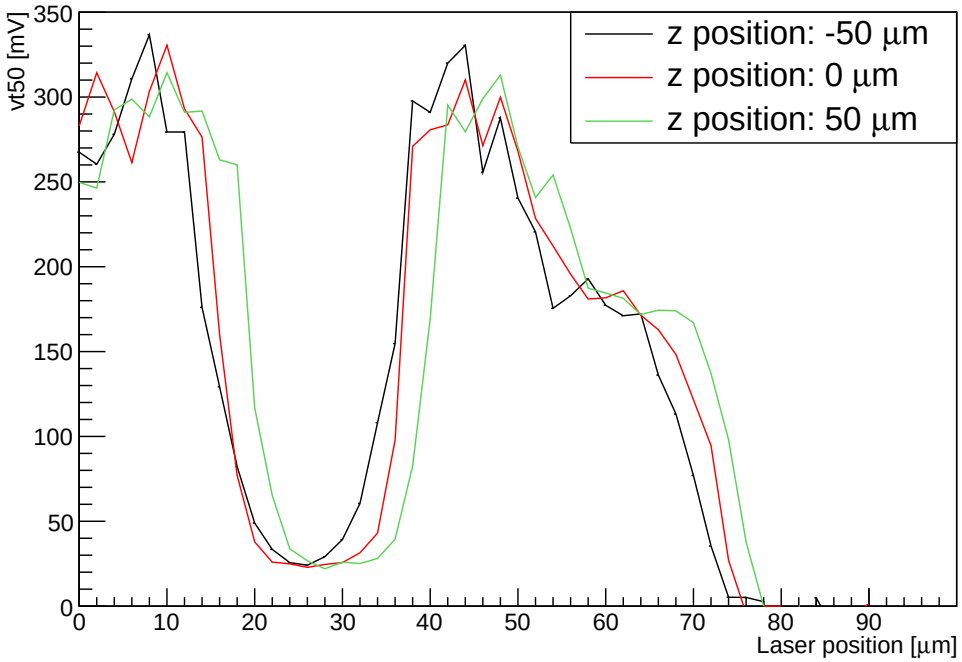

Figure 4.3: The check of laser focus, the best position is 0 μm

correctly set, the bias voltage is not high enough or by property of red laser which does not penetrate the silicon deep enough. All these reasons are based on the fact that in interstrip position close to the surface there is almost no electric field. Because of these characteristics electrons are not able to drift fast enough to catch the detector readout.

But the sum of all the strips shown an interesting behaviour: on some spots the sum is smaller than the response from one strip. It looks like when laser goes from one strip to another, the first strip shows negative response when laser points to another strip. By negative response it is meant the signal that is smaller than the pedestal and it cannot be properly measured.

Fortunately, SCTDAQ has got a feature that artificially raises pedestal using trimming file. Trim file is originally used to smooth pedestal. But in this case this feature comes in handy - the pedestal was raised as much as possible, so the whole negative charge would be visible. Note: after raising pedestal the new 3PG measurements had to be done, since the offset has changed.

Vacuum

When turning on and off the vacuum pump, the module naturally moves a little. How much does it move can be seen in the figure 4.5, where the three measurements were done turning off and on the vacuum pump. All measurements were with bias voltage 80 V, temperature 15°C and y axis laser step of 2 μm. The first measurement was done before turning off the whole setup before the night. The second measurement was done the next day when it was turned on again. Third measurement was done during the day when the pump was off for a few seconds. Between 1st and 2nd measurement there can be seen a movement

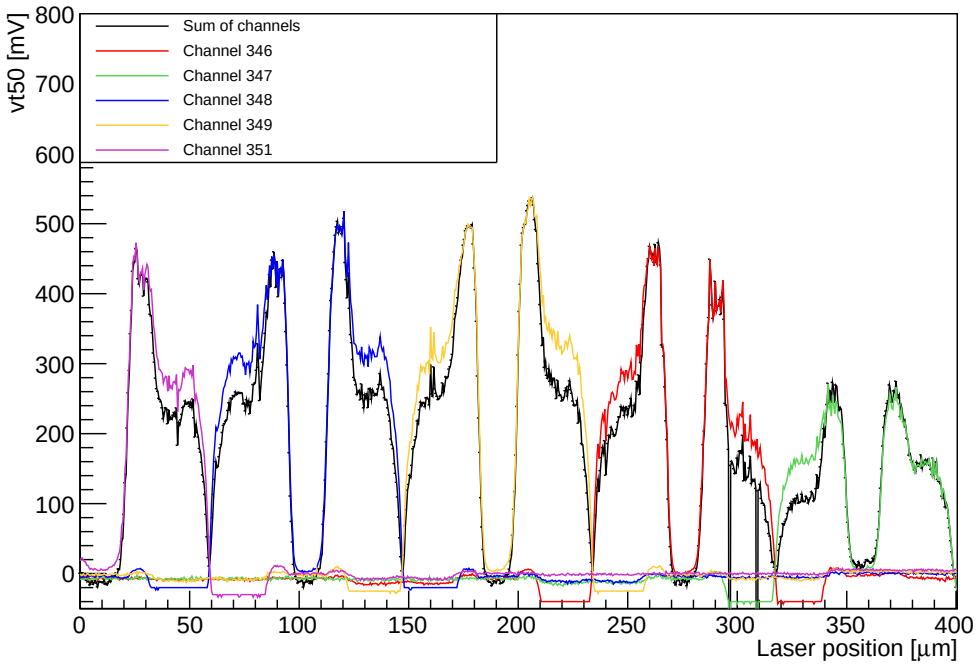

(a) vt50 vs. laser position

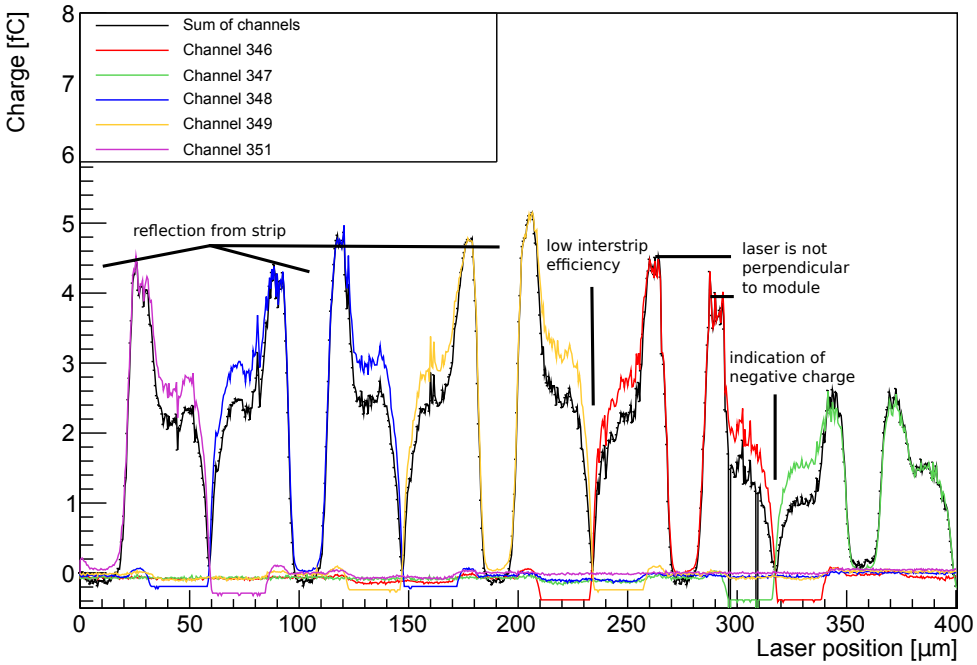

(b) charge vs. laser position

Figure 4.4: Fine scan, one with vt50 and the other with charge on y axis. The second graph shows described features: the laser reflection is visible, low response in the middle of two strips, laser not perpendicular to the module and on some spots the sum is smaller than the response from one strip (indication of negative charge).

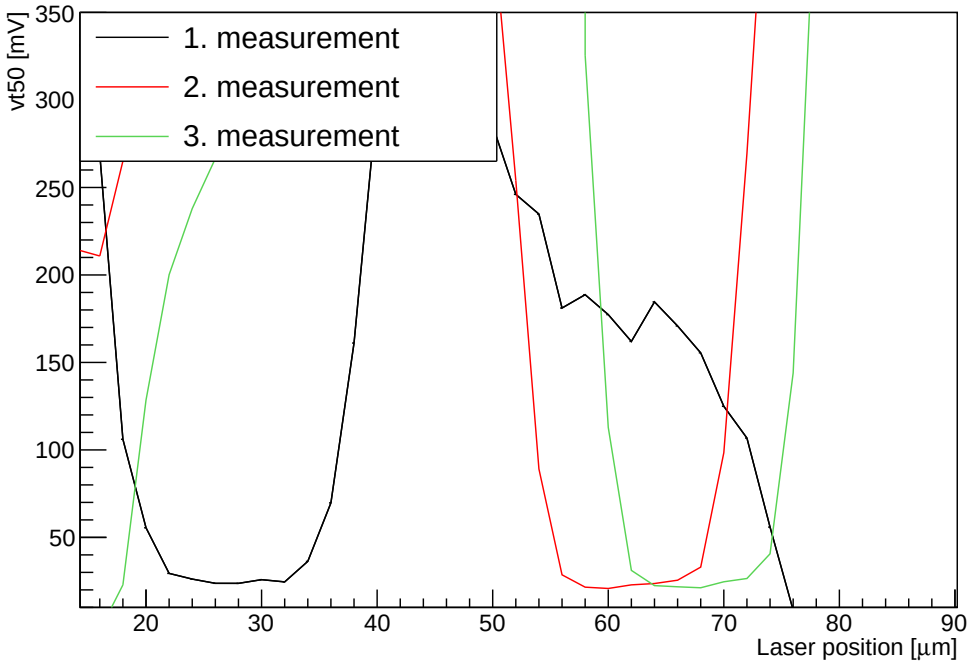

Figure 4.5: Movement of module when turning on and off the vacuum pump. 1st measurement was done before night, 2nd the next day and 3rd during the day when it was turned off for few minutes

of module approximately 35 μm. And between 2nd and 3rd measurement there is smaller movement because the pump was turned off for a short time. Note: the laser was for the all three measurements at the same range of position.

Timing scan

In the figure 4.4 the lower response in the middle of two strips was observed. One of the reasons could be bad timing between laser pulse and the readout. The timing scan was done with y laser movement 0-200 μm with step of 0.2 μm, temperature 15°C and bias voltage 80 V. The original delay was set to 4750 ns; the measured delay range was 4720-4820 ns with step of 10 ns. The result is in the figure 4.6. Its behaviour is the one that is expected, for the certain range of delay all the signal from laser is readout and with delay closer to the edges the lesser (until none) of the signal is readout. The original delay is situated in the good timing plateau which is 4750-4800 ns. The conclusion is that the timing is not the reason for the signal loss.

Higher bias voltage

The next reason for the lower response between strips could be low bias voltage, which can be lifted from 80 V to 100 V. The higher voltage was not possible because of the current. The measurement was done for the y axis laser movement 0-200 μm, step of 2 μm and temperature 15°C. The result is showed in the figure 4.7. The higher bias did not reduced the signal loss.

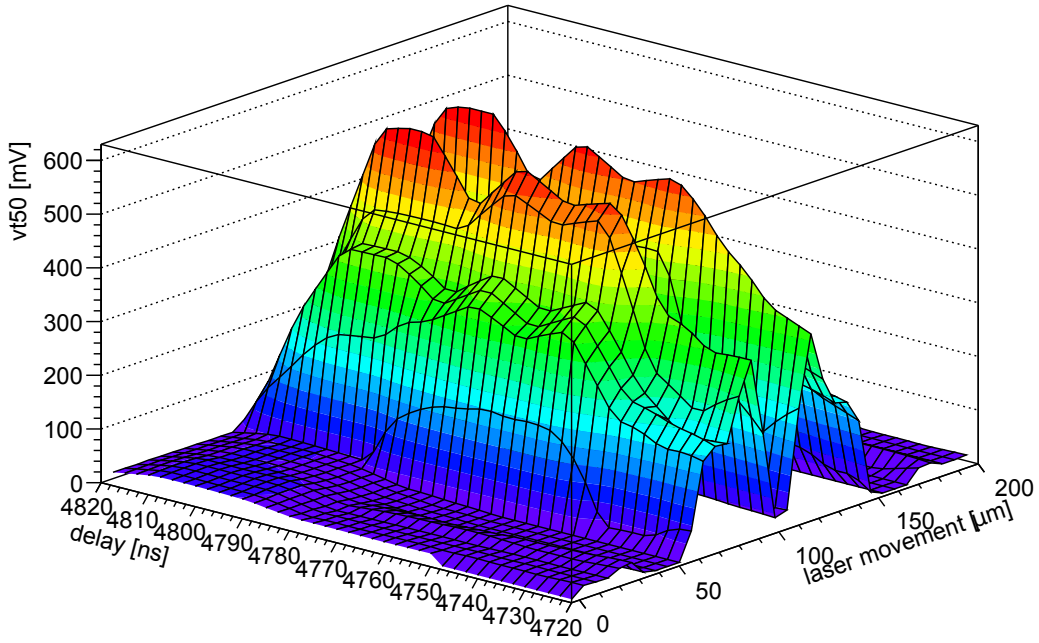

Figure 4.6: Timing scan for module from Freiburg, the shown result is for channel 348. Good timing plateau is 4750-4800 ns

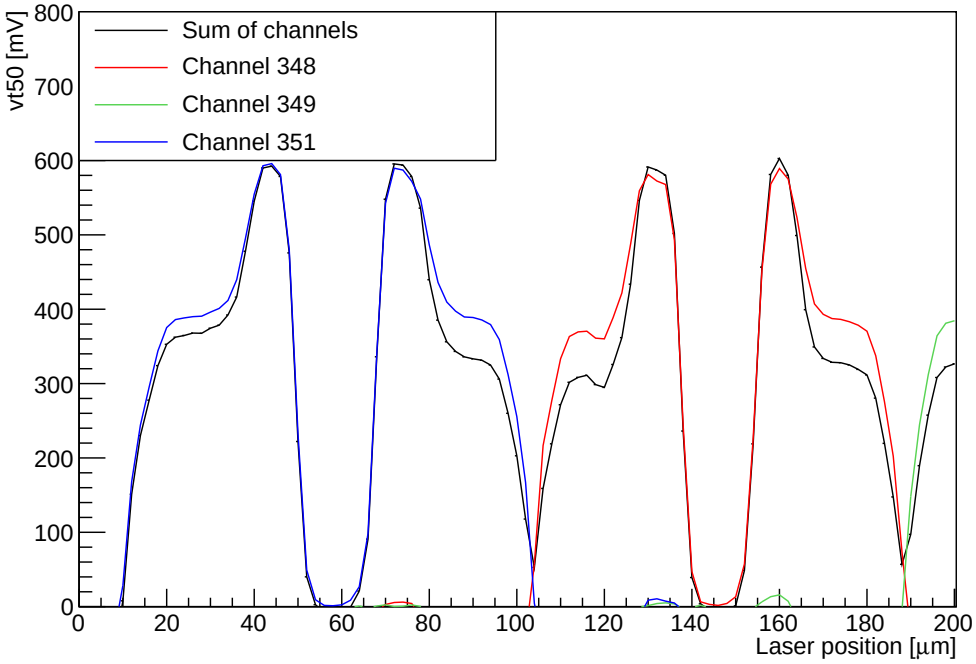

Figure 4.7: Scan with higher bias 100 V

Interstrip scan with trim file

After investigating reasons for the low response in the middle of two strips, the pedestal was artificially raised to investigate the negative part in the figure 4.4. As it was said before, the pedestal was raised by trim file. The pedestal was raised from the original around 30 mV to the highest pedestal as possible around 120 mV. The scan in axis y was done with laser position 0-200 μm, step of 2 μm, temperature 15°C and bias voltage 80 V. The result can be seen in the figure 4.8.

In the figure can be seen again a reflection on the strip, a low response between two strips and also the better view on the negative charge. The decrease in the negative part of the graph is greater than in the graph without using trim file, because with lower pedestal the negative part was only partially visible. That means that the difference between the response in the channel and in the sum of channels is much larger.

The possible explanation for the negative charge is induction in the circuit. Between two strips the AC coupling [1] is present and in the end there is conductor, which behaves like RC circuit. Because the derivation is present, from positive part of pulse it becomes bipolar.

Cluster size

From the graph 4.8 two graphs for cluster size properties were created. The maximum cluster size possible is 3, because in the measurement only three strips were present.

The first graph in the figure 4.9 shows an average cluster size for set threshold and for uniform laser impact point distribution across the sensor. The threshold range for this graph was 0-240 mV with step of 2 mV. It can be seen that there are 2 drops: one around 0.1 fC and the other around 2.3 fC. The first drop corresponds to the threshold where no strips show signal between two strips. The other drop corresponds to the threshold where only part of the strip show signal.

The second graph in the figure 4.10 shows a cluster size for each laser position. There are three graphs present, each for one interesting threshold: 0.043, 2 and 3 fC. Threshold 0.43 fC is where interstrip response is still visible, 2 fC is when the whole strip is visible and 3 fC when the part of the strip disappears. For the threshold 0.043 fC can be seen that there are some laser positions where the cluster size is 3. That is because the threshold is too low that the noise interrupts with signal. For thresholds 2 and 3 fC maximum cluster size is 1, because with these thresholds only one strip at the time is hit. The position range for 2 fC is larger than for 3 fC which is expected, because of the response drop for strip edges.

The reflection of the laser makes the result graphs biased. It is only an optical effect and does not occur when the real particles are detected. It means that data had to be modified to account for the reflection. The response of the laser position where reflection occurs was replaced with the previous response where reflection is not present.

[1] AC coupling or coupling capacitor is an electronic component which links together two AC circuits. AC coupling only passes AC signals, DC is blocked [19].

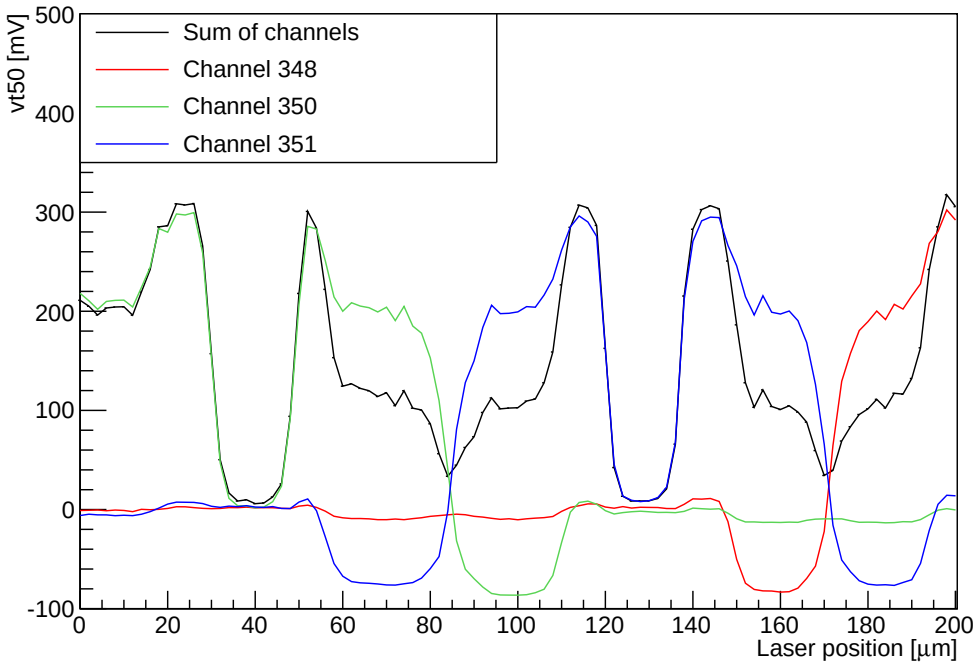

(a) vt50 vs. laser position

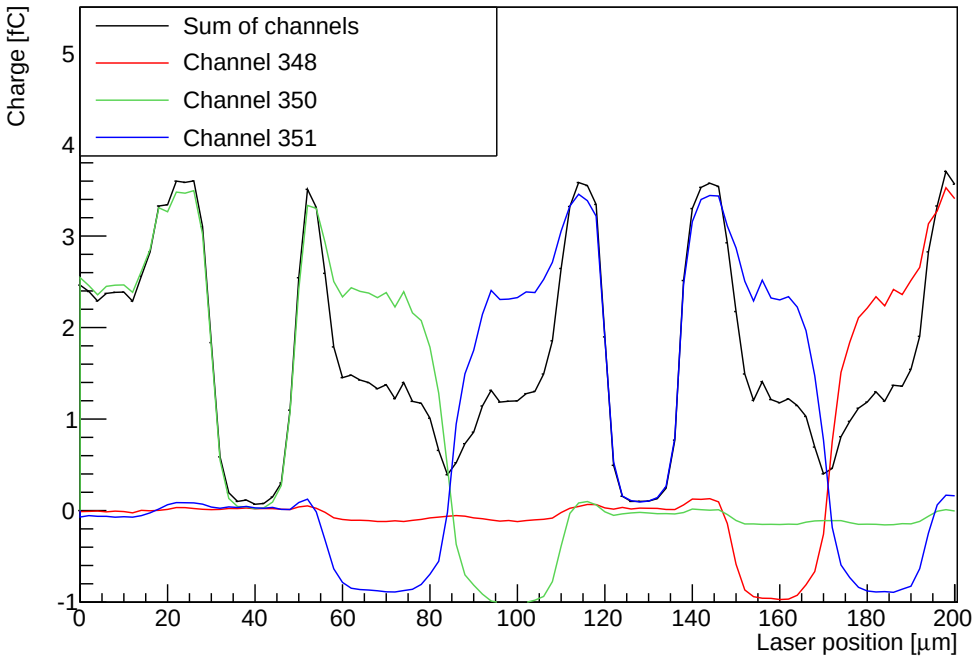

(b) charge vs. laser position

Figure 4.8: Scan with trim file, the negative charge is visible

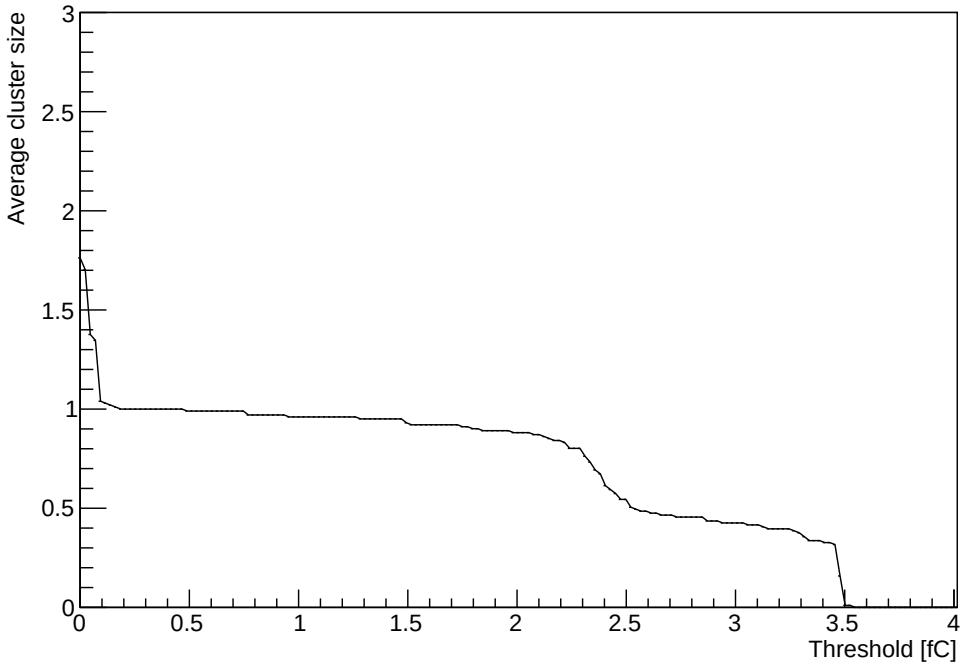

Figure 4.9: Average cluster size vs. threshold for the module from Freiburg. There are two drops in average cluster size. The first around 0.1 fC correspond to the loss of response in interstrip region. The other drop around 2.3 fC corresponds to the loss of response on strip edges.

Timing scan in one laser position

After the discovery of the negative charge, the timing behaviour of the negative charge was measured. In the figure 4.11 can be seen vt50 and charge vs. delay. It was measured with delay range 4680-4820 ns, step of 10 ns, temperature 15°C and bias voltage 80 V.

The graphs were made from one laser position. But it had to be position where the negative charge occurs. The graph shows three lines, one for the channel where the strip is illuminated, one for non-illuminated channel, where only pedestal remains, and the last one for the channel with negative charge. It can be seen, that the negative charge is present only in small timing range (4720-4770 ns), it is not visible for the whole range of good timing for the signal (4750-4800 ns). That leaves very small timing range where both plateau for module and negative part are present 4750-4770 ns.

4.1.2 Conclusion and results

For the module from Freiburg only measurements with red laser were done. Since this was the first module for laser tests the system was debugged during measurements - mainly focusing laser and using trim file.

After analysing the first measurement it was found that laser was defocused. The next measurement was aimed for focusing the laser. Later the negative charge was discovered and pedestal was raised.

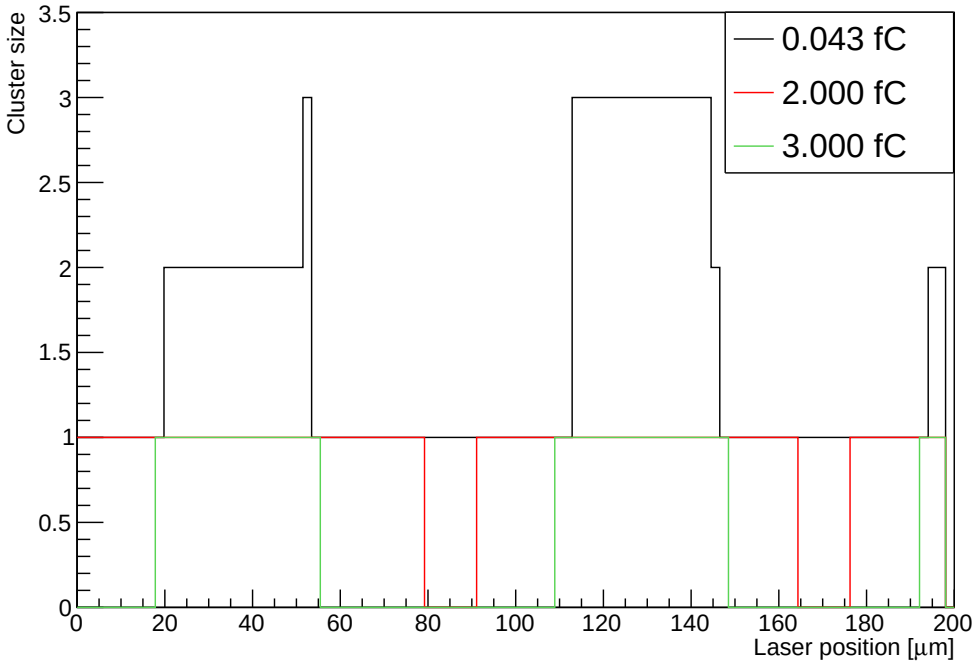

Figure 4.10: Cluster size vs. laser position for the module from Freiburg. Graph shows the dependence for three interesting thresholds where interstrip response and the edges of strips are still visible and where response from the strip edges is not present.

As for the results, the 2D laser scan with laser movement in some range was done. As expected, there was no response due to reflection on the strip, where the light from laser does not get into detecting part of the sensor. What was not expected was wrong order of strips. The reason was wrong bonding algorithm what ended in wrong bonding and order of the strips. Bad bonding cannot be detected with electronic tests.

There was also seen a large signal loss between two strips. The signal between two strips almost drops to the pedestal as can be seen from the cluster size graph in 4.10. The original signal was around 3.5 fC and it dropped to signal around 0.043 fC. This could be caused by many reasons: wrong timing, insufficient bias voltage or by property of red laser which does not penetrate a silicon deep enough. One reason was refuted by our measurement - the timing was right. Regarding the higher bias voltage, it could be only raised to 100 V and the loss did not change. But there is a possibility that with higher bias (not possible with this module) the response would change. With red laser there was also seen negative charge next to the strip. As it was said before the reason for it can be induction.

The result of timing scan confirmed that the original timing was right and there is plateau of good timings for readout of the whole signal. Its size is 50 ns. Also the timing of the negative charge was investigated and the result is that negative charge is easy to miss because it is present in small range of timings with size 20 ns.

At the beginning of the laser tests the macros for automatic measurement were written. Along with them also macros for analysing measured data and

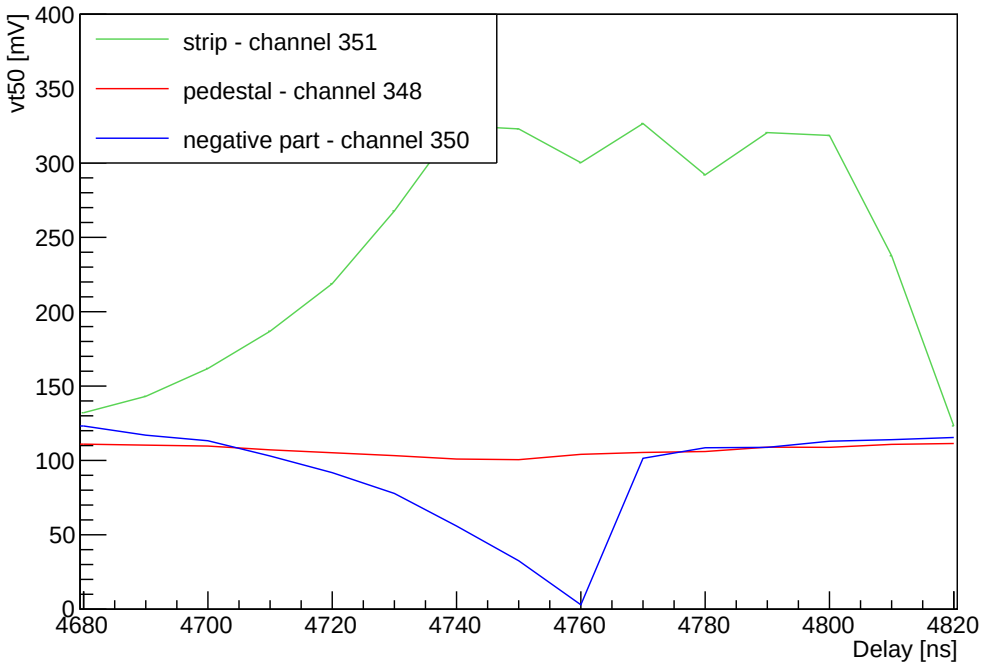

(a) vt50 vs. laser position

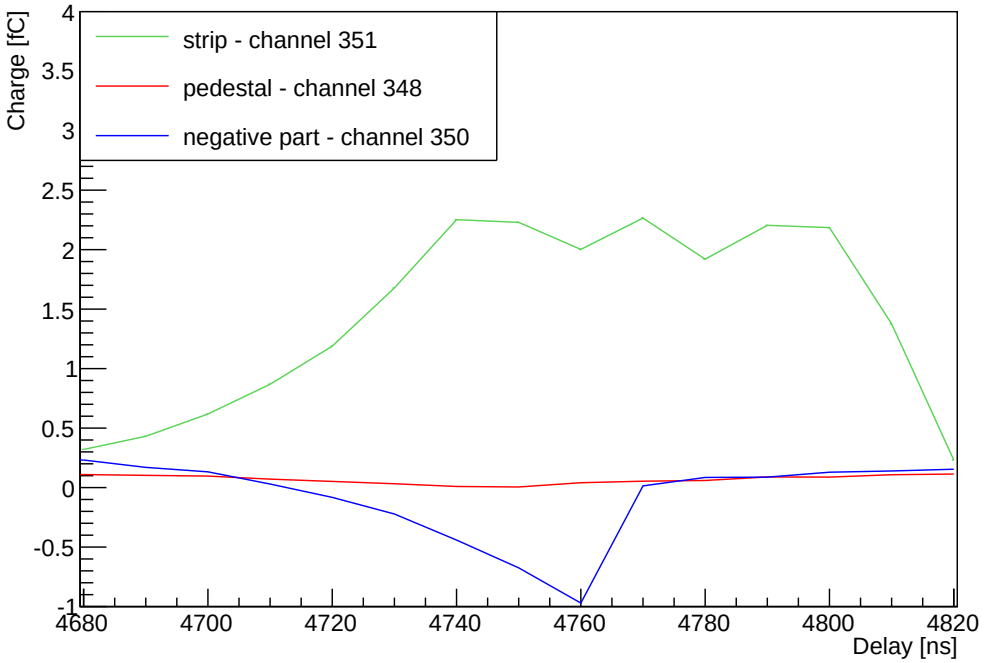

(b) charge vs. laser position

Figure 4.11: Timing scan with trim file for one position of laser. Shown three options for response: channel with only pedestal, with hit strip and with negative charge

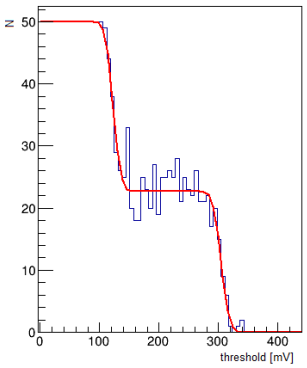

Figure 4.12: Data with custom fit of drop of response with laser

creating graphs were written.

4.2 Module from Zeuthen

For this module both red and infra-red laser tests were done. The tests started with infra-red laser to see another laser at first and then the red laser to compare with the previous module.

All the tests were performed with already focused laser and the use of trim file to be able to see potential negative charge.

4.2.1 Infra-red laser

Double error function fit

After engagement of the new module, a bad readout occurred. At some point while reading out the channel with laser the response dropped to 50%. Because SCTDAQ is programmed to fit error function, the result of the fit was incorrect. The data had to be fitted with sum of two error functions:

$$f(x) = \mathrm{erfc}_1(x) + \mathrm{erfc}_2(x) \tag{4.1}$$

There are 5 fitted parameters: $\mathrm{vt50}_1$, $\mathrm{vt50}_2$, σ_1, σ_2 and $\mathrm{constant}_1$. $\mathrm{Constant}_2$ is defined with number of inserted pulses: $\mathrm{constant}_2$ = nTrigs - $\mathrm{constant}_1$.

The correct vt50 is $\mathrm{vt50}_2$ of the second error function. The data and custom fit can be seen in the figure 4.12. SCTDAQ fitted vt50 somewhere in the plateau in 50% response.

The difference between SCTDAQ's fit and custom fit can be seen in the figures 4.13, 4.14 and 4.15. The measurements were done for three bias voltages: 30 V, 80 V and 140 V, with temperature 15°C, y axis laser position 0-200 μm and step of 2 μm. There can be seen major difference between SCTDAQ's vt50 and the real one. The higher bias voltage is, the bigger the difference between these two fits is present. It is related to connection between bias voltage and the sensor response (vt50).

The problem of the response drop seemed to be caused by readout cable's bad connection. Future tests do not show any response drop.

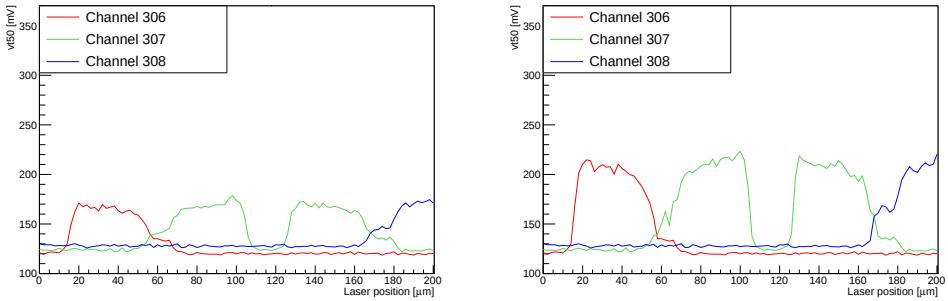

(a) Without custom fit (b) With custom fit

Figure 4.13: The difference in fits of the y-position scan for 30 V

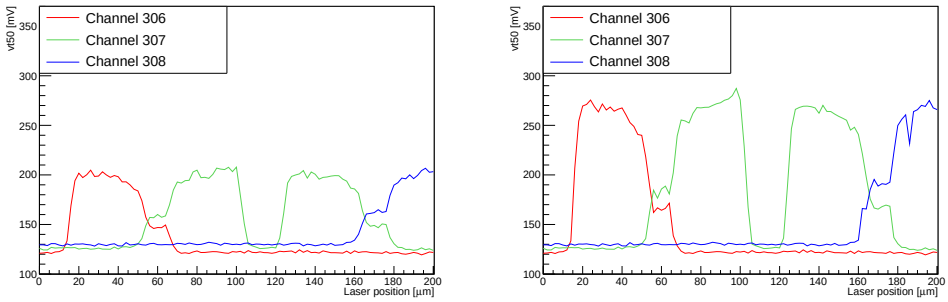

(a) Without custom fit (b) With custom fit

Figure 4.14: The difference in fits of the y-position scan for 80 V

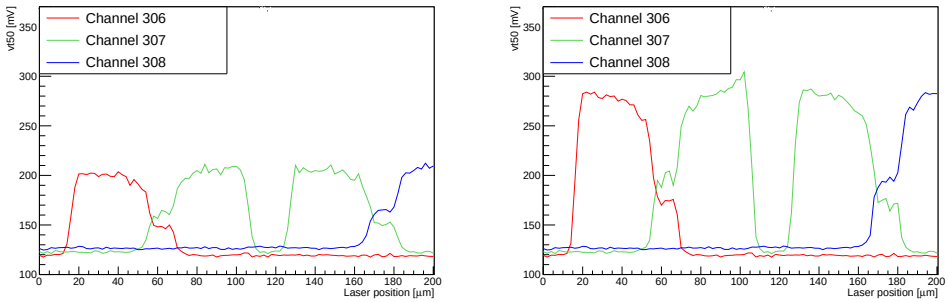

(a) Without custom fit (b) With custom fit

Figure 4.15: The difference in fits of the y-position scan for 140 V

Fine interstrip scan

The next measurement was fine y-position scan with range 0-400 μm and step of 0.5 μm. The bias voltage was 130 V and temperature 15°C. In the figure 4.16 can be seen again a reflection from the strip and a signal loss between two strips, a drop to 1/3 of the original response. The loss is not as big as in the previous module and red laser, but it is present. Negative charge does not seem to be present. But the absence of the negative charge could be caused by timing - like in the case of the previous module where the negative charge was present only for short time interval. That means that the timing scan is essential for the next measurement.

Timing scan

The timing scan was done for delay 4700-4820 ns with step of 20 ns. The bias voltage for this measurement was 120 V with temperature 15°C and laser position was 0-200 μm with step of 2 μm. The result can be seen in the figure 4.17.

From this dataset the graph of timing in one laser position was created. Again, the position had to be chosen where the negative charge might occur. It was 100 μm. The graph of delay vs. vt50 is in the figure 4.18. It can be seen that the negative charge is not present for any delay.

Perpendicular laser position

As it was said in the previous section, the laser is not perpendicular to the module, it is slightly inclined - about 1°. For better result the right perpendicular position for the laser was measured. The range of angle was $\pm 2°$ from the original position 90° with step of 0.5°. The y axis laser position was 0-250 μm with step of 5 μm. The results can be seen in the figure 4.19. There is one graph for each angle for better overview.

In the figure one can see that edge positions are too shifted, because the signal is higher on one side of the strip than on the other side. The best angle is between 90° and 89.5°.

Finer angle scan with step of 0.25° was done in this region. All the other conditions were the same. The result is in the figure 4.20. The best laser angle is 89.75°.

Fine interstrip scan in perpendicular position

The angle was set to the perpendicular position and then a fine y-position scan was done. The conditions were: temperature 15°C, bias voltage 120 V and range 0-400 μm with step of 0.5 μm. The result is shown in the figure 4.21. The left and right side of the strip are in the same height comparing to the previous fine scan in 4.16.

Cluster size

Like for the previous module cluster size graphs were made. The graphs were created from the graph in the figure 4.21. The first graph, average cluster size

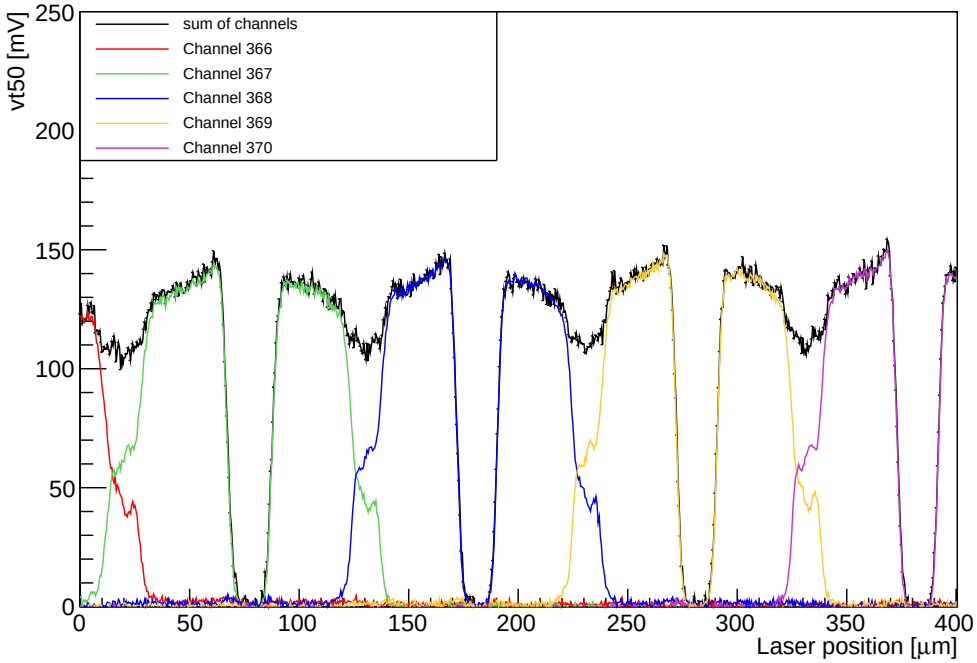

(a) vt50 vs. laser position

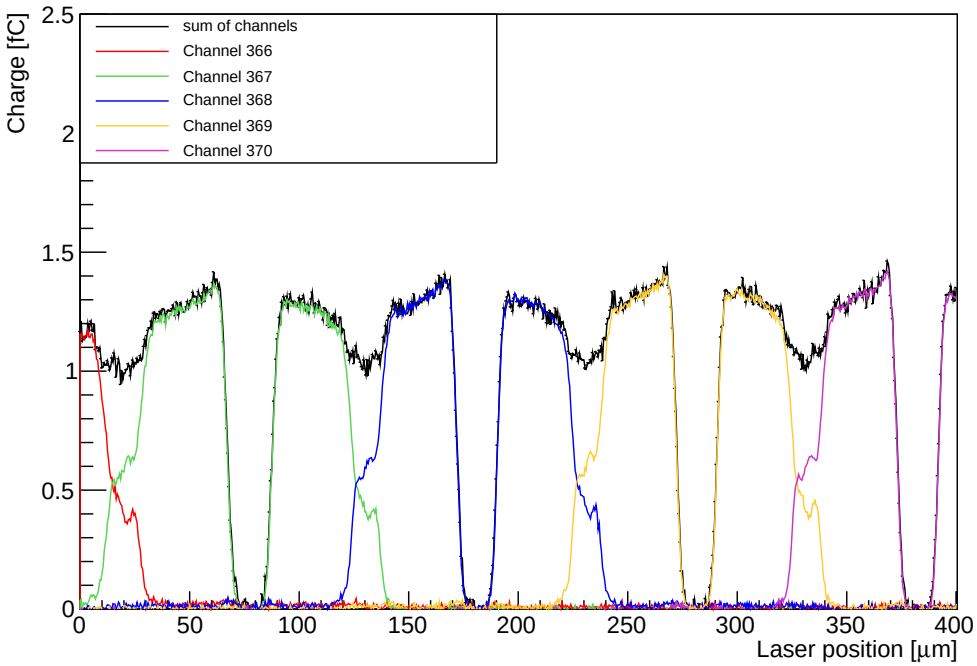

(b) charge vs. laser position

Figure 4.16: Fine scan with infra-red laser, no negative charge is visible

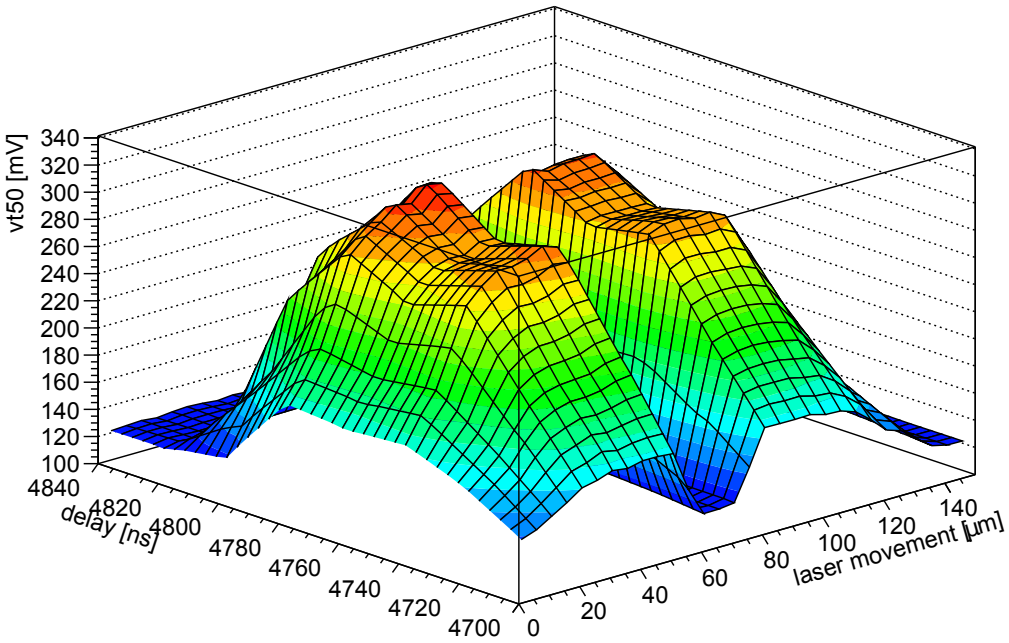

Figure 4.17: Timing scan with infra-red laser, in the figure only range up to 140 μm. The shown result is for channel 307

vs. threshold, is in the figure 4.22. Used threshold range was 0-120 mV with step of 1 mV. There is one drop around 0.3 fC which corresponds to a response loss from an interstrip region.

For the second graph only two interesting thresholds were drawn: 0.2 and 0.8 fC. The threshold 0.2 fC is where interstrip response is still visible and 0.8 fC is without interstrip region but still with a response from the strips.

4.2.2 Red laser

Because the setup for the module from Zeuthen was debugged on IR laser, only y-position scan and timing scan was done with this laser. All the measurements were done with bias voltage 120 V and temperature 15°C.

Interstrip scan

At first, delay was set to 4800 ns from the previous measurements with IR laser. At this delay a y-position scan was done with range 0-200 μm and step of 2 μm. The result is in the figure 4.24. The negative charge seems not to be present as it was with IR laser. It still could be present though, just this timing makes it not visible.

Timing scan

Then the timing scan was done to find out whether the negative charge occurs or not. The measurement was done for delay 4680-4820 ns with step of 20 ns.

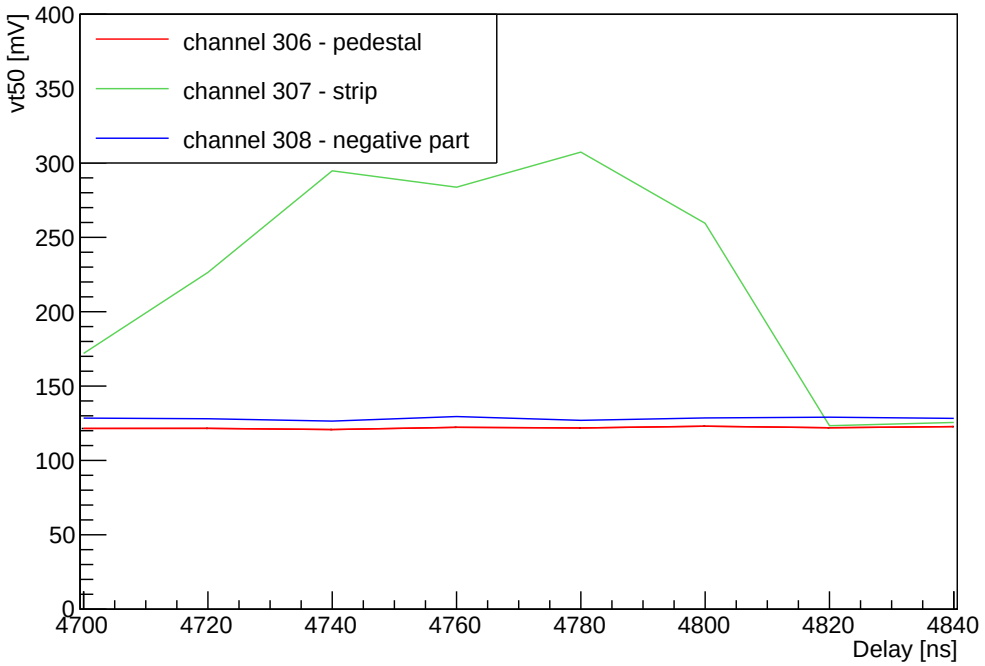

(a) vt50 vs. laser position

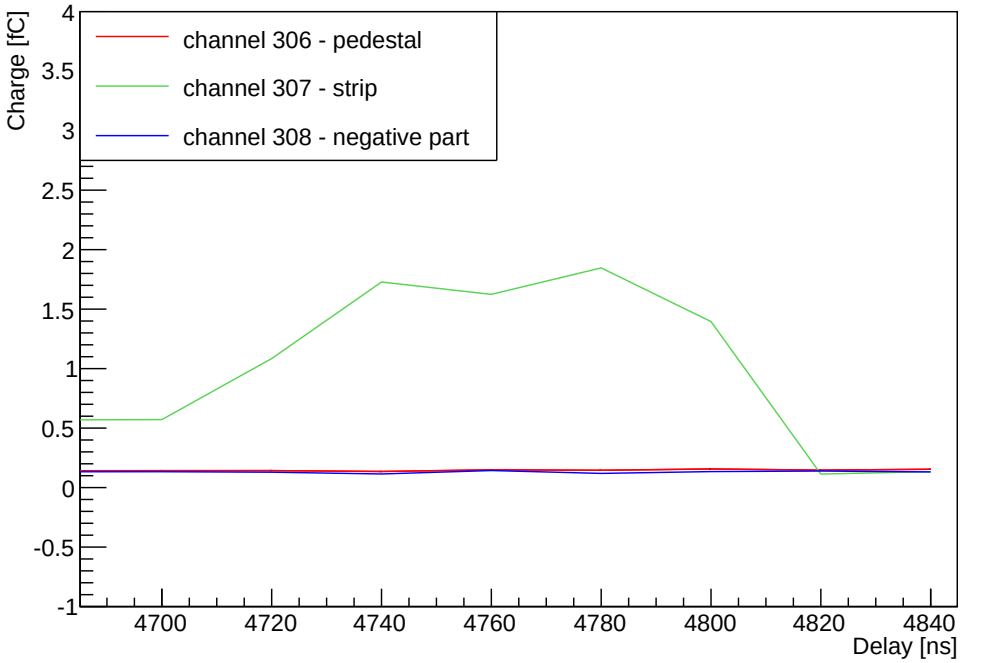

(b) charge vs. laser position

Figure 4.18: Timing scan for one position of laser. Shown three options for response: channel with only pedestal, with hit strip and with negative charge. No negative charge is visible

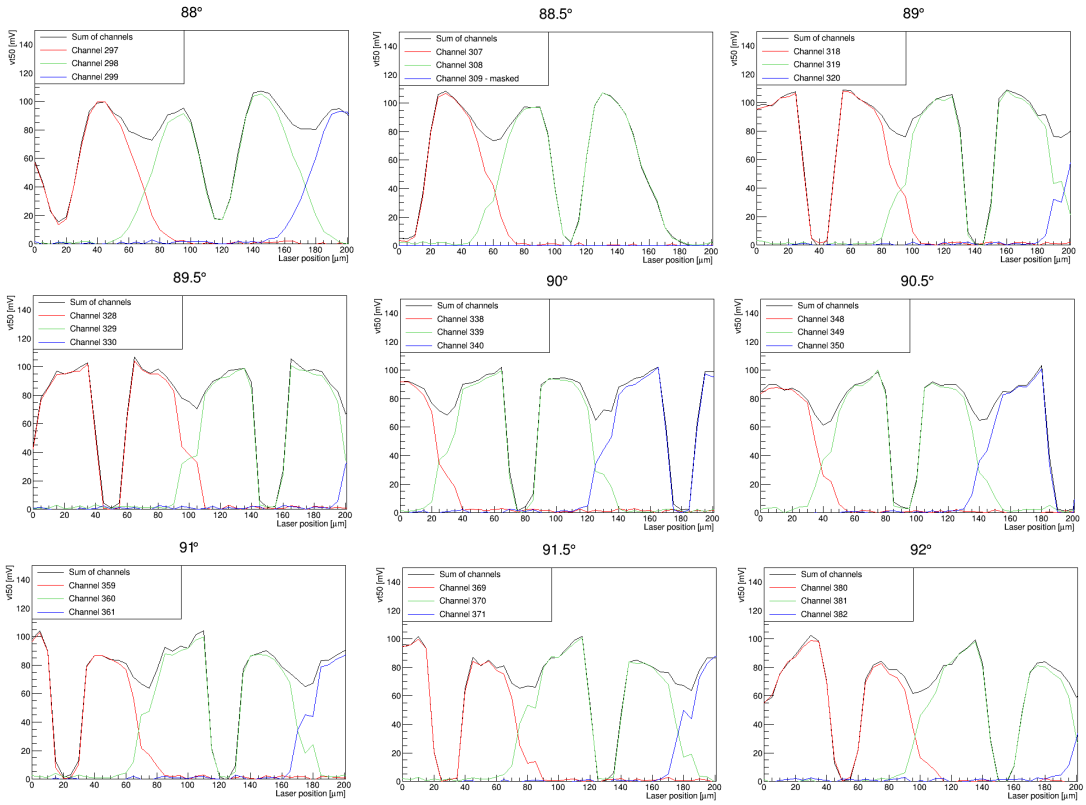

Figure 4.19: Angle scan, for 88.5° one strip was masked (response hidden by SCTDAQ). The best angle is between 90° and 89.5°

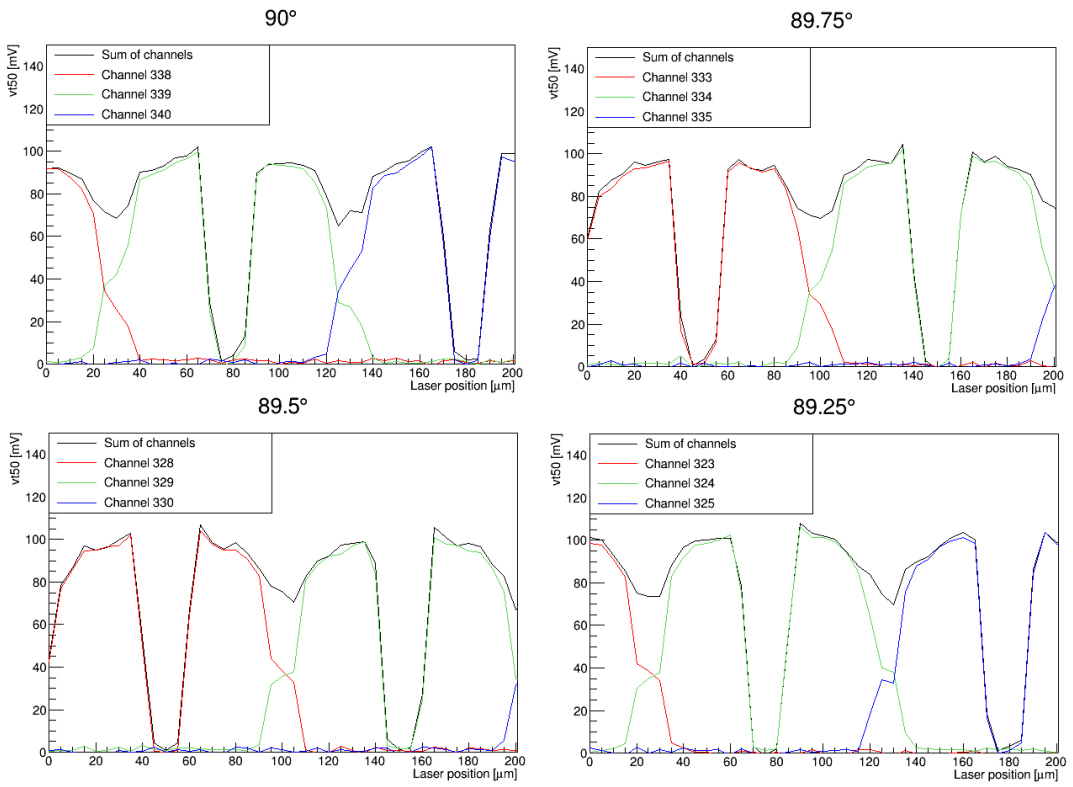

Figure 4.20: Finer angle scan, the best angle is 89.75°

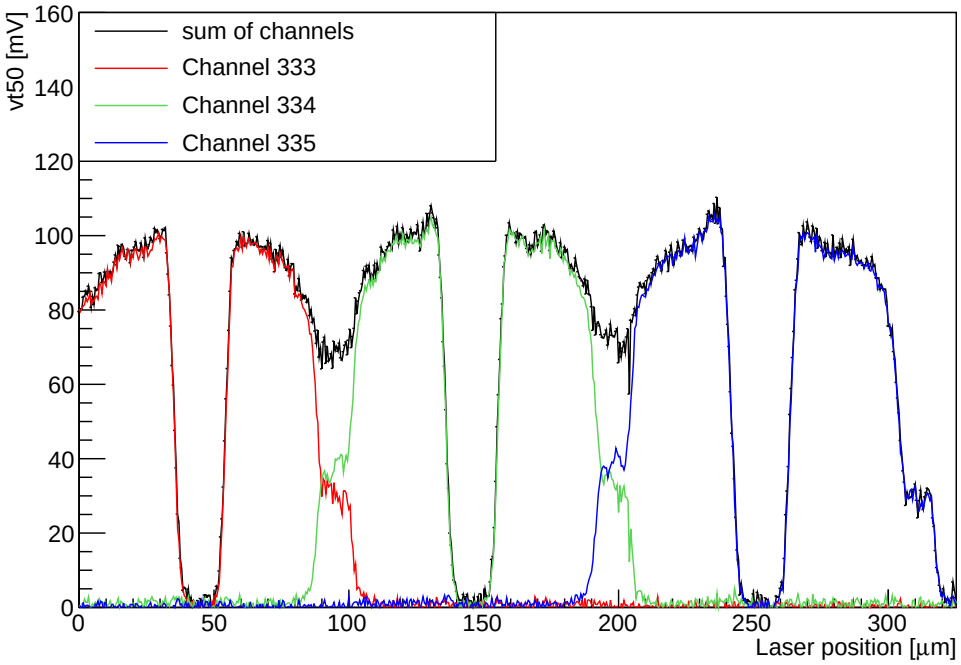

(a) vt50 vs. laser position

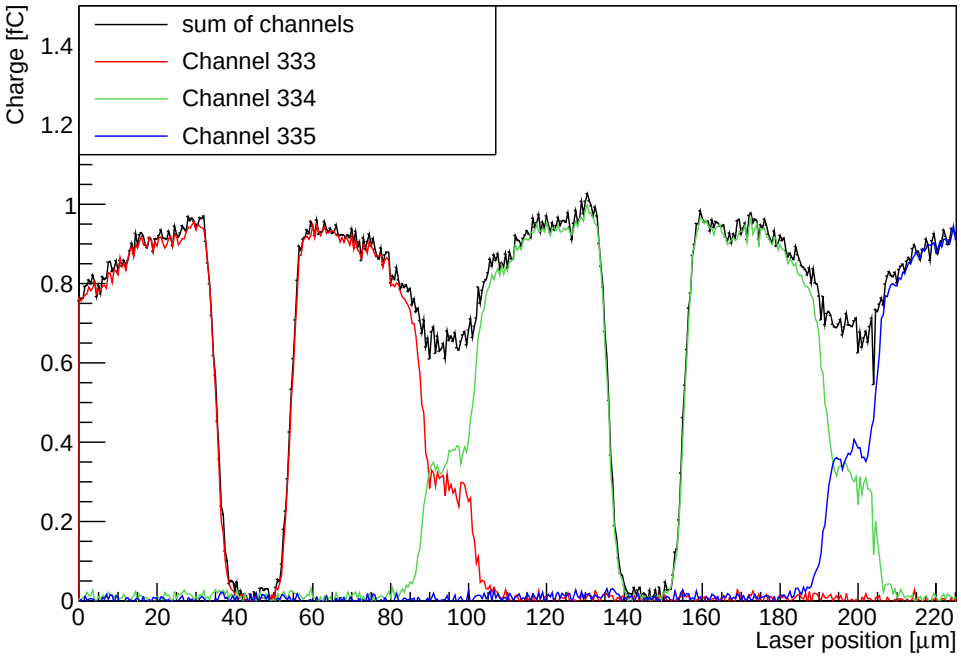

(b) vt50 vs. laser position

Figure 4.21: Fine scan in perpendicular position, the left and right side of the strip are in the same height

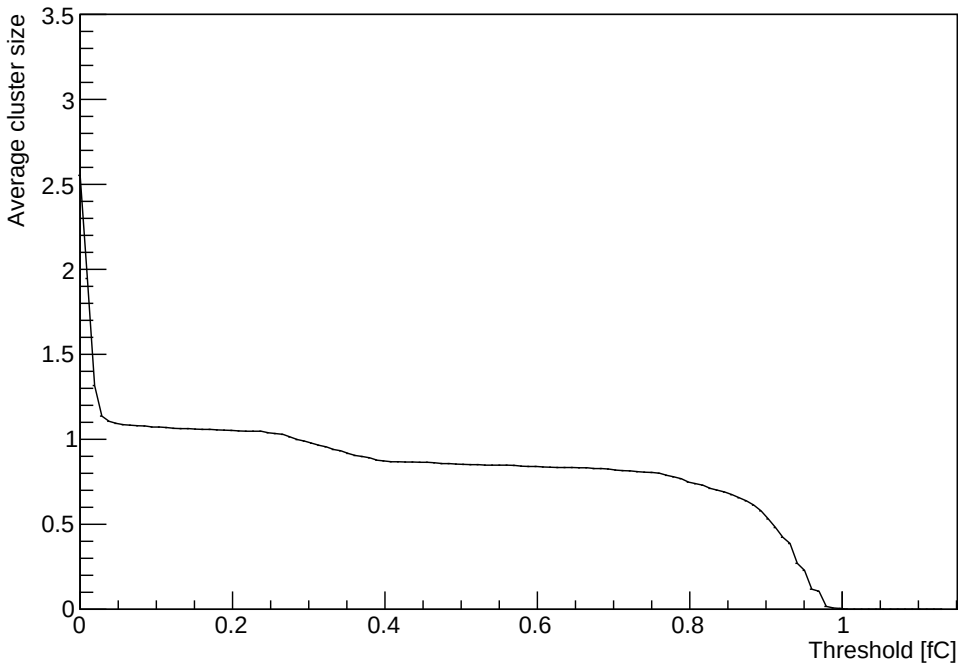

Figure 4.22: Average cluster size vs. threshold for module from Zeuthen and IR laser. There is only one drop around 0.3 fC that corresponds to loss of interstrip response.

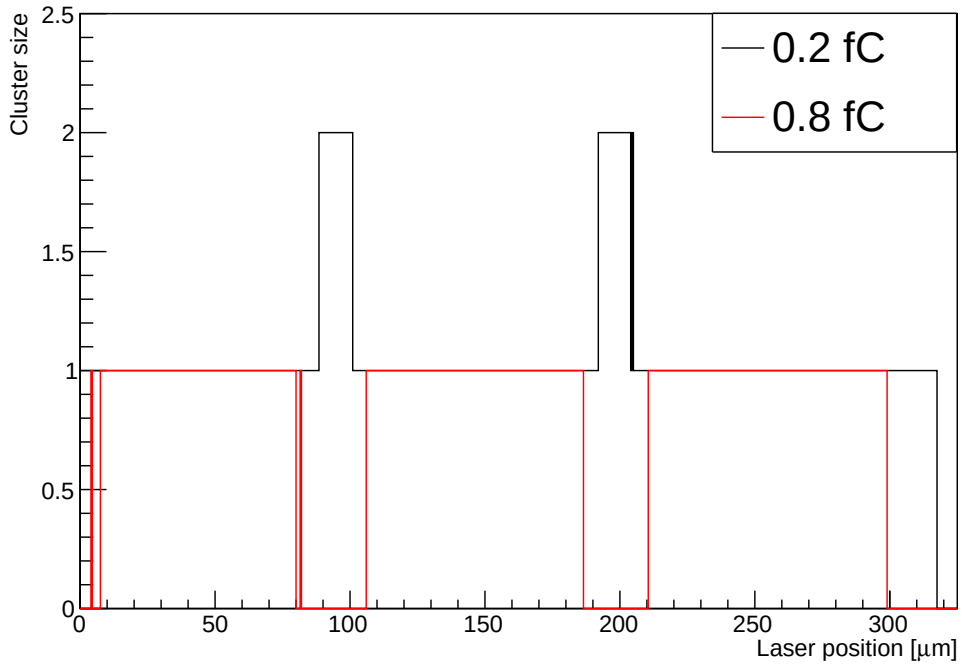

Figure 4.23: Cluster size vs. laser position for module from Zeuthen and IR laser. The dependence is shown for two interesting thresholds where the interstrip response is and is not visible.

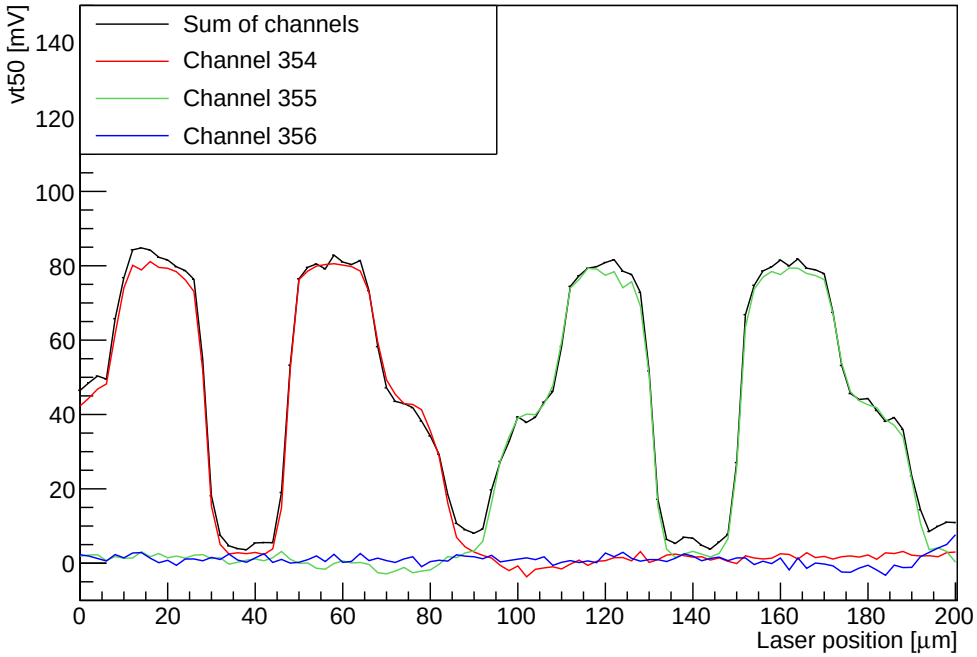

Figure 4.24: Scan with red laser, delay 4800 ns. No negative charge visible

The 3D graph can be seen in the figure 4.25 and one laser position graph in the figure 4.26.

It can be seen that the negative charge is present for all range of good timing which is 4740-4800 ns. The lowest negative charge is in delay 4760 ns and its size is around 10 mV/0.1 fC.

Fine interstrip scan

A fine y-position scan was done for range 0-400 μm with step of 0.5 μm and delay 4760 ns, where negative charge occurs and it is the most visible. The result is shown in the figure 4.27.

In this graph one can see that the negative charge is present and also there is a signal loss between two strips is much higher than for the IR laser, it almost overlaps with pedestal.

Cluster size

From the previous graph in the figure 4.27 the graphs describing cluster size properties were made. The graphs are shown in figures 4.28 and 4.29. In the first graph there are two drops, one for the loss of interstrip response almost at the beginning of x axis and the other for the loss of response on the edges of the strips around 0.5 fC. Interesting thresholds in the second graph are 0.03, 0.45 and 0.8 fC. The first two thresholds show cluster size right before each drop described in the first graph. Threshold 0.8 fC shows cluster size after the second drop.

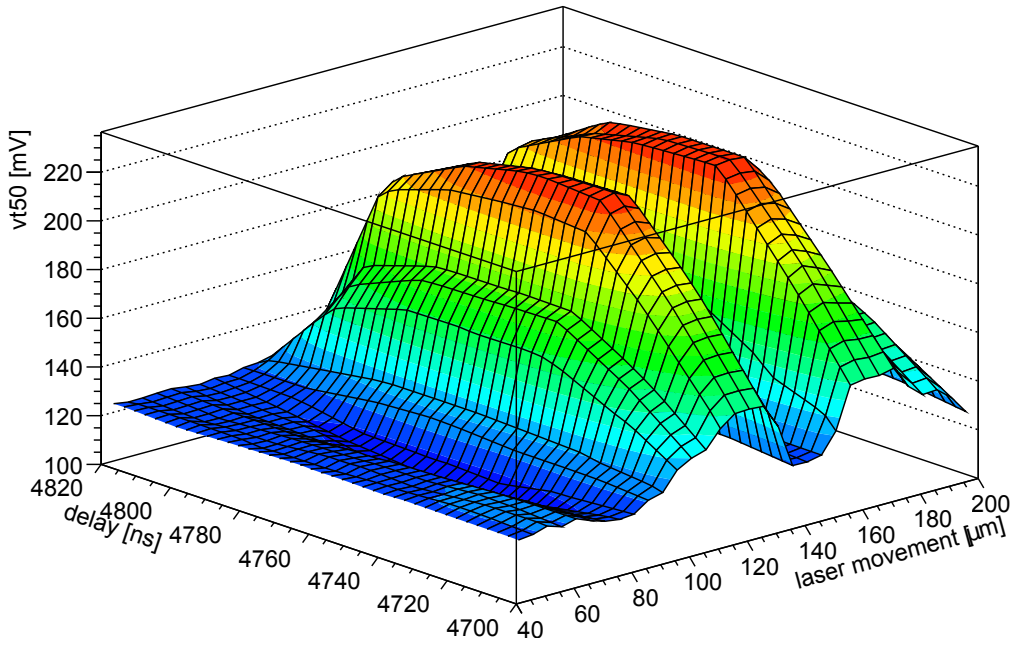

Figure 4.25: Timing scan with red laser, channel 355, negative charge occurs

4.2.3 Conclusion and results

With the module from Zeuthen both red and infra-red laser tests were done. Because setup was for the most part functional from the measurements on the previous module from Freiburg, the tests were done immediately with focused laser and with use of the trim file. The artificial pedestal was again around 120 mV. The first measurements were done with infra-red laser, later with red.

At first, the problem with response drop occurred. When strip was illuminated by the laser, the response dropped at first to 50% and then to 0. Data analysis from the measurement with this feature had to be corrected and data had to refit by sum of two error functions.

The reason for response drop was poor contact of data cable. When the connection was adjusted, the shape of s-curve was correct without any unexpected drops.

The y-position scan in the figure 4.16 did not discover any negative charge and the drop between two strips was present, but not that large, only to 1/3 of original response (original response 0.9 fC dropped to 0.3 fC). Search for the negative charge continued with timing scan because, as it was seen with the module from Freiburg, it could be present only for small range of timing. Even the timing scan did not find any negative charge.

The last measurement with infra-red laser was finding the perpendicular position of the laser. After evaluation of data laser was rotated by motion stages by -0.25° from the original position 90°.

With the laser in perpendicular position, a fine y-position scan was measured. The response from left and right side of strip had the same value.

With the red laser was again inspected negative charge. At first it was not

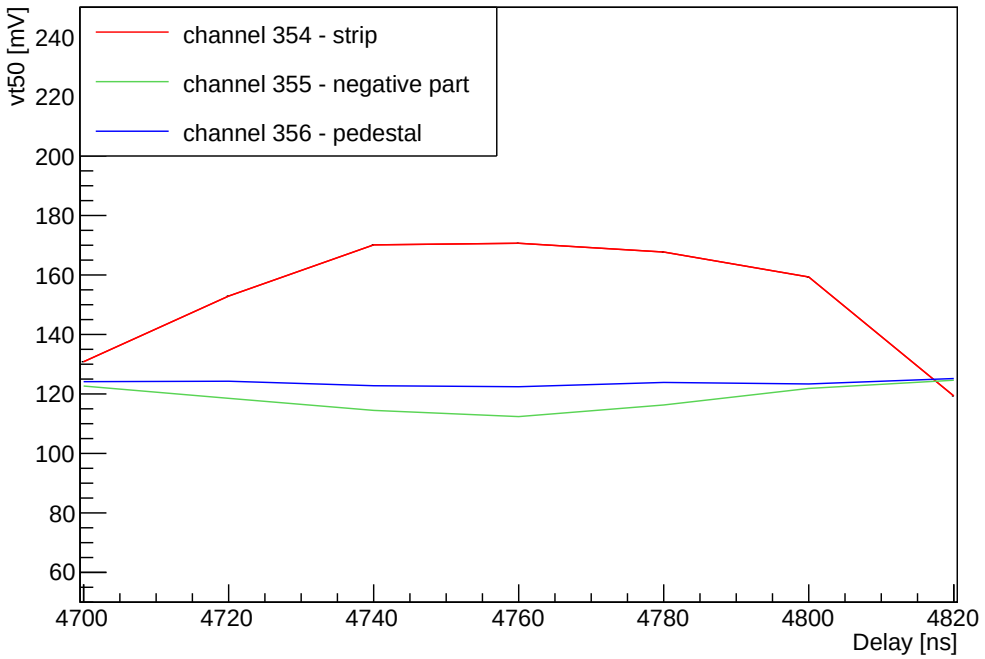

(a) vt50 vs. laser position

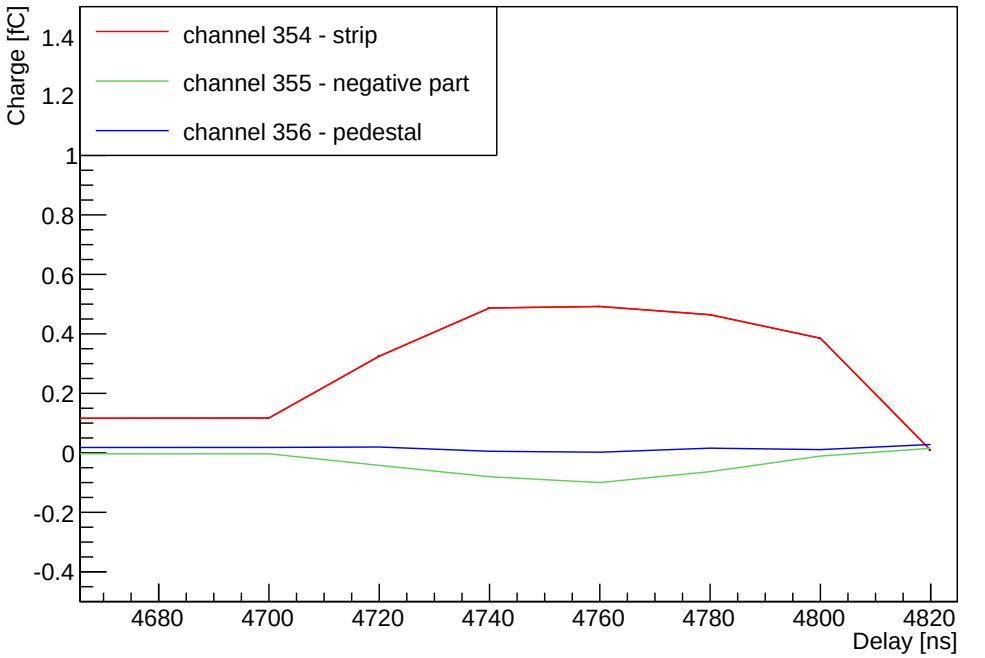

(b) charge vs. laser position

Figure 4.26: Timing scan with red laser for one position of laser. Shown three options for response: channel with only pedestal, with hit strip and with negative charge. Negative charge is visible

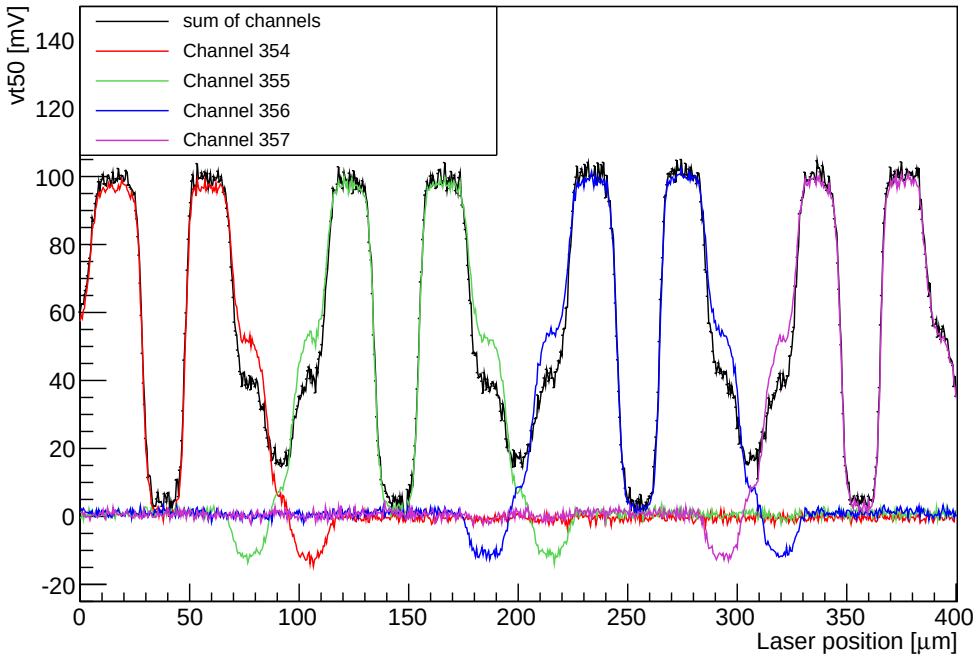

(a) vt50 vs. laser position

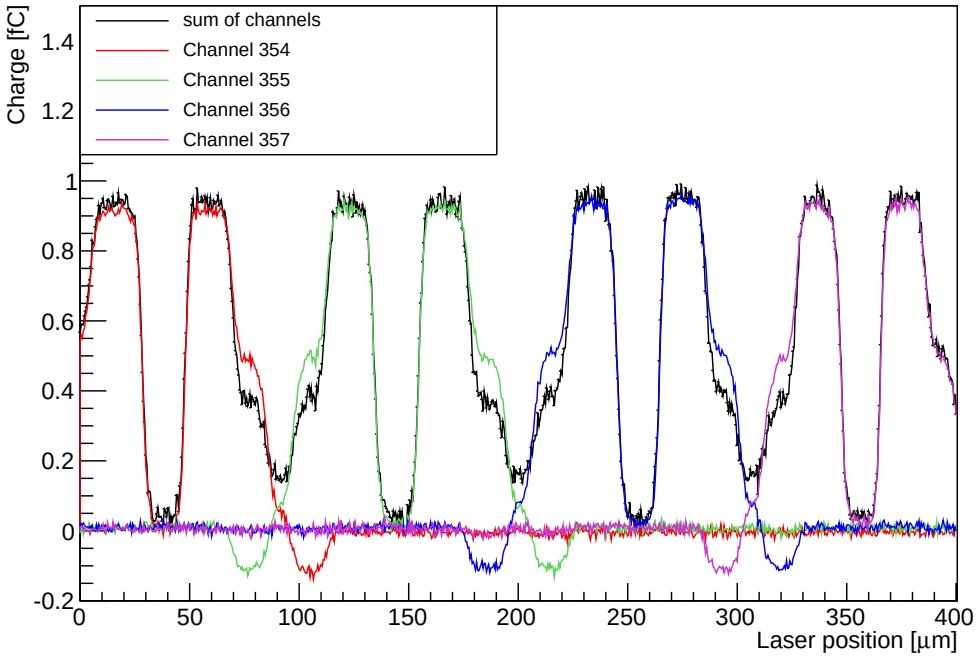

(b) vt50 vs. laser position

Figure 4.27: Fine scan with red laser. Negative charge and signal loss between strips are present

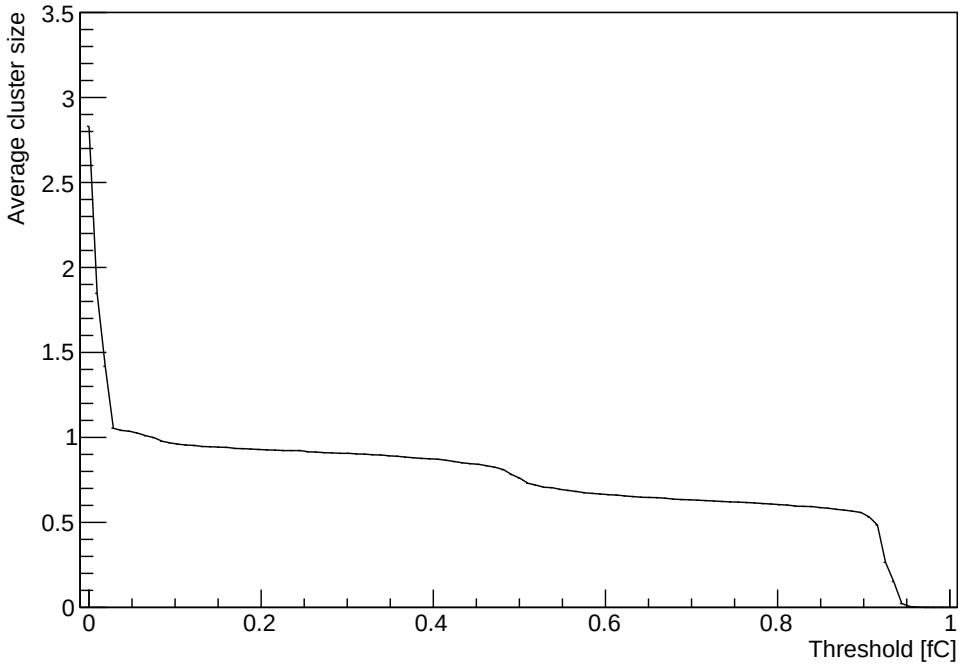

Figure 4.28: Average cluster size vs. threshold for module from Zeuthen and red laser. Two drops are visible: one at the beginning where the loss of interstrip response occurs and the other around 0.5 fC where a loss of response on strip edges is present.

visible, but with the right timing it appeared. Negative charge was present almost for the whole range of delay.

Interstrip efficiency was significantly reduced compared to infra-red laser. The size of the response drop was to 1/30 of the original signal (original 0.9 fC dropped to 0.03 fC).

4.3 Summary and comparison

For the laser tests two modules were available. The tests were done with both red and infra-red lasers. For measuring and analysing data the macros were written.

During the first tests a bad bonding was discovered on the module from Freiburg. It could not be discovered by electric tests, only with laser tests.

After laser tests some interesting properties were discovered: firstly a very small interstrip efficiency, secondly the presence of negative charge on the neighbouring strips.

The efficiency between two strips was much smaller for measurements with red laser than with infra-red laser. For the red laser the drop was almost to the pedestal level; for the infra-red laser the drop was to 1/3 of the original response. Larger drop for red laser can be explained by properties of red and infra-red laser. The red laser penetrates only s surface of a detector, which means that carriers in the interstrip region near surface are not fast enough to catch readout

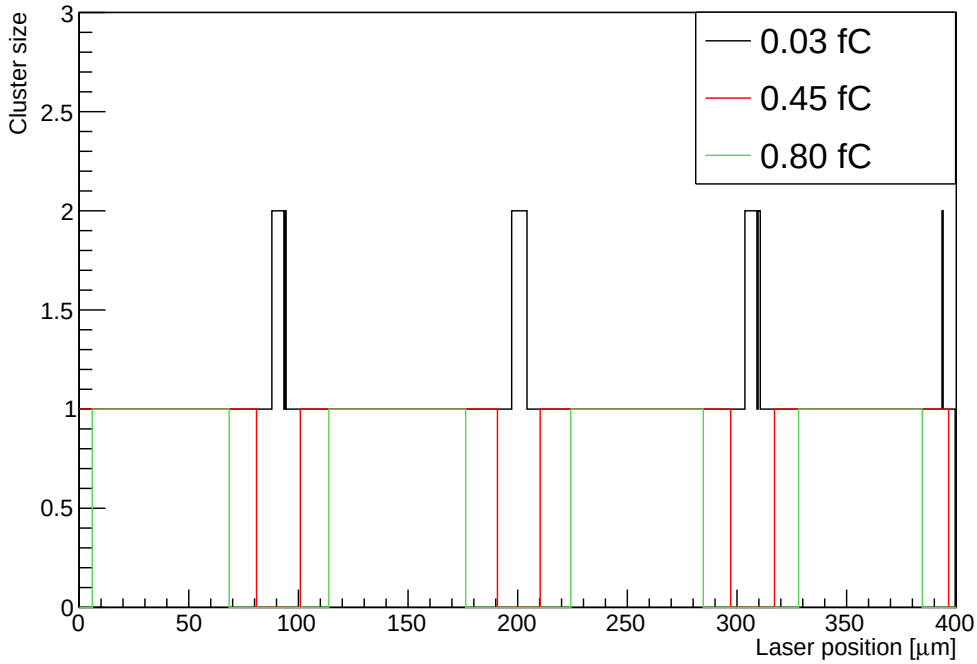

Figure 4.29: Cluster size vs. laser position for module from Zeuthen and red laser. Graph shows the dependence for three interesting thresholds where interstrip response and the edges of strips are still visible and where response from the strip edges is not present.

window. But infra-red laser penetrates much deeper thus there are more carriers in interstrip region deeper in silicon, not just only near surface. Thus the efficiency is better for the infra-red laser.

The negative charge was discovered with red laser (present for the neighbouring strips), with infra-red laser it was not observed at all.

The reason for negative charge could be induction in the circuit. A possible explanation for its presence only during measurement with red laser is that red laser does not penetrate deep into silicon, it hits only the surface. Thus the properties of electronics play bigger role in the result. In infra-red laser results there could be some negative charge present, but since infra-red laser penetrates much deeper into silicon, the electronics barely influence the result.

These were the results for the module from ATLAS Upgrade. In 2002-2006 module tests for the original ATLAS experiment were done. It included electronic, beta source, laser tests and also series of thorough tests before installing to ATLAS. The following text will shortly compare results from the previous laser tests.

The previous laser tests were done also in IPNP. In the figure 4.30 there is a result from laser test with infra-red laser [20]. In the graph there is the same response behaviour as it was in current infra-red laser tests. There is a reflection from the strip an also a decrease of the signal in the middle of two strips. The signal loss is to half of the original response. That means that both tested modules for ATLAS Upgrade in this thesis have got insufficient interstrip response.

In the graph from 2002-2006 there can be also seen a signal share to the

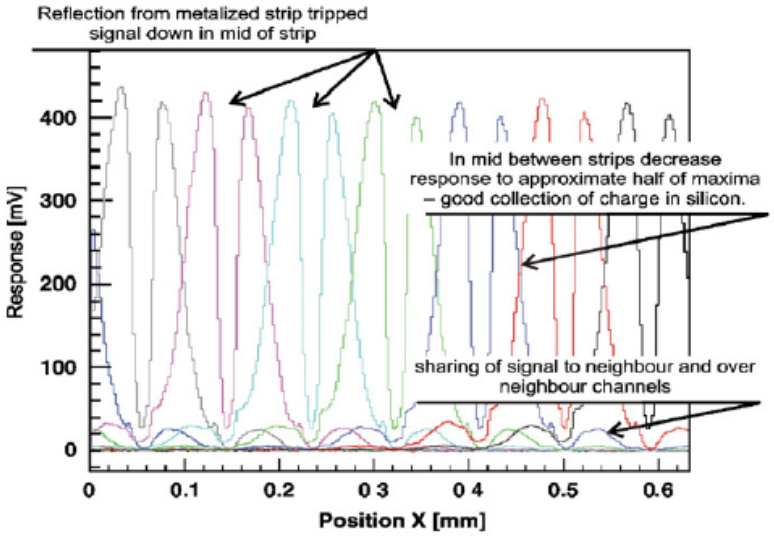

Figure 4.30: The results from laser tests with infra-red laser in 2002-2006 [20]. Figure shows features identical with ATLAS Upgrade modules: a reflection on the strip and efficiency drop in the interstrip region. Charge sharing was not observed for current modules

neighbouring strip. This feature was not observed using infra-red laser with ATLAS Upgrade modules.

In the figure 4.31 there is a result from laser tests with red laser. In the graph one can see a negative charge that occurred in the current laser tests.

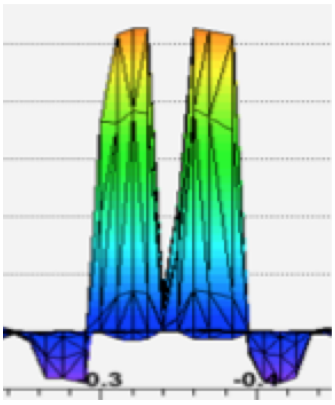

Figure 4.31: The results from laser tests with red laser in 2002-2006 where the negative charge occured [21]

5. Use of the macros

All the data, analysis and graphs were, as said before, created using custom ROOT-based macros. All macros are located on server IPNP30 in following directory: `/home/meszarosova/macros`. In this chapter the use of these macros will be explained.

Along with these macros manual for using the apparatus for future testing by future users will be created. The .pdf file will be located also on IPNP30 server in the same directory.

In this chapter the basic use of measuring and analysing macros will be described. The further description will be included in .pdf file and also some description is written inside the macros as a comment.

5.1 Macros for measurement

For the measurement two macros were written: one for the movement of the laser in one direction and the other for the movement in two directions.

The macro called `Threshold_Scan_LM.cpp` was written for laser movement in one direction. The properties of the measurement are set inside the macro after opening it in a viewer. In the section Input variables there are variables that can be set:

- `direction` - with this variable the laser movement axis is set. The axes described in the chapter 4 have the numbers: 1 for x axis, 2 for y axis and 3 for z axis.
- `distance` - one step in mm of the laser is set. The sign of the variable sets the direction of the movement. For example: for y axis minus was for the raise of the number of channels and for z axis minus was for laser to move down (closer to the module).
- `pocet` - number of threshold scans which will be measured.
- `VThr_start` - sets the start value of threshold in mV.
- `VThr_stop` - sets the last value of threshold in mV.
- `VThr_step` - sets the step of threshold in mV.
- `Ntrigs` - sets number of triggers (constant of s-curve).

The macro for two axes movement is called `Threshold_Scan2D_LM.cpp`. The properties of the measurement are also set inside the code in section Input variables. The principle is the same with a few more variables:

- `direction1` and `direction2` - has the same function as direction in the previous macro. `direction1` sets the first axis of laser movement and `direction2` the second axis.
- `pocet1` and `pocet2` - has the same function as the variable `pocet`.

- `distance1` and `distance2` - has the same function as the variable `distance`.

With a macro the measurement can be run. At first, it is needed to be placed where SCTDAQ's files are installed in the directory \macros. Then it is needed to run SCTDAQ and with command `.x Threshold_Scan_LM.cpp` and the measurement will start with set properties.

Both macros also create .txt log file which will be located after measurement on local computer in `e:\sctvar\log\`. In the file there will be date and time of the start of the whole measurement. Then the start of the each threshold scan with its run and scan number, begin time and the position of axis/axes.

5.2 Macros for analysis

For the analysis of the measured data four macros were written: two for creating graphs for threshold scan and two for timing scan.

The first macro is called `TS_1D.cpp`. Inside the macro in the section Input variables the properties of the run is set and the macro will create two graphs: vt50 vs. laser movement and charge vs. laser movement. For the right result the file with offset and gain have to be included. The example .txt file is in the same directory.

The second macro has the same function as the first but with difference that it analyses data from 2D threshold scan and the result graph is 3D graph. It is called `TS_2D.cpp`. It only plots vt50 (not charge) thus the file with gain and offset is not necessary. It only creates vt50 because 2-axis scan was used only to measure laser focus.

For analysis of the timing scan there were written two macros: one for creating 3D graph and one for creating graphs for one laser position. They could be put together into one macro, but for better overview they were made into the directory separately. The first is called `timing_scan.cpp` and its function is to create a 3D graph with axis x, y and z: laser position, delay and vt50 of set channel number.

The second macro is `timing_scan_onepos.cpp` which creates two graphs of timing in one laser position, one for vt50 and the other for charge. The graph is for one defined laser position and for three strips which show the timing distribution in strip, pedestal and negative charge (if present).

Conclusion

For the conclusion, the results from this master thesis will be summarized.

At first, CERN, LHC and current ATLAS detector were briefly described. Then ATLAS Upgrade was described with the focus on inner detector (ITK) and its strip silicon detectors. The description was aimed to the differences between current ATLAS and future ATLAS Upgrade. The biggest change will be sole use of silicon components.

Then the principle of silicon detectors was explained. At first characteristics of semiconductors were explained: band structure, carrier transport and generation. Later the principle of strip and pixel silicon detectors and the logic of readout from detectors were described. Knowledge of the principle of silicon semiconductor detectors was essential for the next parts of thesis, to be able to understand the results of measurements.

Before showing any results, the process of measurements had to be described. This part was written more thoroughly, because it was important to understand how the whole setup works. In this part of thesis there was described a motivation for doing these kinds of tests on the prototype modules, special (clean) room for measurements and the reasons for need of this kind of room. There was also described what kind of equipment is necessary for doing laser test and how does each component work and communicate with each other. This part consists of many photos for better image of the whole layout.

The tests were done with two modules, one from Freiburg and one from Zeuthen. They were prototypes of end-cap strip silicon detectors for ATLAS Upgrade. As for the results, the first tests were done without using any external source to measure noise of the modules. The next results were from the laser tests, for module from Freiburg with red laser and for module from Zeuthen with both red and infra-red lasers.

To summarize the tests, the following tests were done in all cases: y-position laser scans with finer laser step to see response of the module in strip region and region between two strips. The second test was timing scan where timing between laser pulse and detector readout was changed. Along these tests which were done on every module and every laser, other measurements were done to debug and improve the system. There were measurements for laser focus, test to see how does module moves when vacuum is turned off and on and measurement to set laser into perpendicular position.

After first measurements on Freiburg module it was discovered that the module has got bad bonding. This error could not be detected using only electrical tests.

As for other results from laser test that were discovered, two most important will be mentioned.

The results from the red laser show very inefficient response from the region between two strips, it almost reaches a pedestal. With the infra-red laser it is more efficient, but still the drop was to 1/3 of the original signal. This behaviour responds to properties of the lasers, where the red laser penetrate only the surface of detector. It means that electrons are not fast enough in this region. But the infra-red laser penetrates much deeper thus the interstrip efficiency is better.

During the tests with red laser a negative charge was discovered. It appeared in the results from both modules with red laser, but not in the result from infra-red laser. The possible explanation could be induction in the circuit. The reason why it is seen with the red laser is again in the penetration depth. Since the red laser penetrates only the surface, the result gives information mainly about electronics. And vice-versa, infra-red gives information mainly about detector, where the negative charge could be present, but it is overwhelmed with the response from the sensor.

The last part of thesis contains a description of the macros that were written for measuring, analysing and creating graphs.

In conclusion, with laser tests there was seen some expected behaviour such as reflection from the strip. But also there were discovered some new features such as small efficiency and negative charge.

The system for the laser tests is functional and ready to be be used by someone else. There was also created a method (macros) for measuring and analysing data. All measurements including measuring using macros, analysing of measured data and creation of the graphs in this thesis were done by the author.

The whole setup is currently used for a laser tests with another reading hardware ATLYS (similar to HSIO used during laser tests in this thesis). The whole method that was created during this thesis will be also used for the future laser tests with more prototypes.

Bibliography

[1] *About CERN*, online [28.11.2015]: http://home.cern/about

[2] *Restarting the LHC: Why 13 TeV?*, online [18.2.2016]: http://home.cern/about/engineering/restarting-lhc-why-13-tev

[3] *Map of CERN Accelerator Complex*, online [29.11.2015]: https://upload.wikimedia.org/wikipedia/commons/b/ba/Cern-accelerator-complex.svg

[4] *ATLAS fact sheet*, online [2.12.2015]: http://www.atlas.ch/pdf/ATLAS_fact_sheets.pdf

[5] *Transition Radiation Tracker (TRT)*, online [1.12.2015]: http://atlas.ch/inner_detector3.html

[6] Jochem Snuverink: *ATLAS Muon Spectrometer: Commisioning and Tracking*, 2009, ISBN-13: 978-90-365-2912-9, available online [1.12.2015]: http://www.nikhef.nl/pub/services/biblio/theses_pdf/thesis_J_Snuverink.pdf

[7] ATLAS Collaboration: *Letter of Intent Phase II Upgrade*, CERN-LHCC-2012-022, LHCC-I-023, 2012, p.1-5 a 57-104

[8] Zdeňka Broklová: *Vyhodnocení účinnosti a kvality polovodičových stripových detektorů pro detektor ATLAS LHC CERN*, master thesis, Charles University in Prague, 2003.

[9] Gerhard Lutz: *Semiconductor Radiation Detectors*, Springer Berlin Heidelberg New York, 1999, ISBN 978-3-540-71678-5, p.1-108

[10] Zdeněk Doležal: *Polovodičové detektory v jaderné a subjaderné fyzice*, text to lecture, available at [18.2.2016]: http://www-ucjf.troja.mff.cuni.cz/~dolezal/teach/semicon/semi_p.pdf

[11] *PHYS 11.4: Quantum physics of solids*, online [29.12.2015]: http://www.physics.brocku.ca/PPLATO/h-flap/phys11_4.html

[12] Jakobs, K.: *Particle Detection and First Physics Results from the LHC, chap. 2.3 Silicon Semiconductor detectors*, online [20.2.2016]: http://portal.uni-freiburg.de/jakobs/dateien/dok/vietnam11d

[13] *Error function*, online [27.3.2016]: https://en.wikipedia.org/wiki/Error_function

[14] Z. Doležal et al.: *Systematic effects in some semiconductor detector tests*, Nuclear Instruments and Methods in Physics Research Section A: Accelerators, Spectrometers, Detectors and Associated Equipment, vol.583, issue 1, p.37–41, 2007

[15] *Peter Kodyš's web pages*, online [12.3.2016]: http://www-ucjf.troja.mff.cuni.cz/~kodys/

[16] *ROOT*, online [5.5.2016]: `https://root.cern.ch/`

[17] Martin Sýkora: *Tests of Semiconductor Detectors in Prague Laboratory*, bachelor thesis, Charles University in Prague, 2015

[18] Carlos Garcia Argos: *Procedure for operating the HSIO DAQ system for single modules in the B180 setup*, electronic communication with Ina Chalupková

[19] *Capacitive coupling*, online [20.4.2016]: `https://en.wikipedia.org/wiki/Capacitive_coupling`

[20] Z. Doležal et al.: *Laser tests of silicon detectors*, Nuclear Instruments and Methods in Physics Research Section A: Accelerators, Spectrometers, Detectors and Associated Equipment, vol.573, issues 1–2, p.12–15, 2006

[21] Z. Doležal, electronic communication